

1 **GISS Model E2.2: A Climate Model Optimized for the**  
2 **Middle Atmosphere. Part 2: Validation of Large-Scale**  
3 **Transport and Evaluation of Climate Response**

4 **Clara Orbe<sup>1</sup>, David Rind<sup>1</sup>, Jeffrey Jonas<sup>2,1</sup>, Larissa Nazarenko<sup>2,1</sup>, Greg**  
5 **Faluvegi<sup>2,1</sup>, Lee T. Murray<sup>3</sup>, Drew T. Shindell<sup>4</sup>, Kostas Tsigaridis<sup>2,1</sup>, Tiehan**  
6 **Zhou<sup>2,1</sup>, Maxwell Kelley<sup>5,1</sup>, Gavin A. Schmidt<sup>1</sup>**

7 <sup>1</sup>NASA Goddard Institute for Space Studies, 2880 Broadway New York, NY 10025

8 <sup>2</sup>Center for Climate Systems Research, Earth Institute, Columbia University, New York NY

9 <sup>3</sup>Department of Earth and Environmental Sciences, University of Rochester, Rochester NY

10 <sup>4</sup>Nicholas School of the Environment, Duke University, Durham NC

11 <sup>5</sup>SciSpace LLC, New York NY

12 **Key Points:**

- 13 • The stratospheric transport circulation is evaluated for the new GISS “high-top”  
14 CMIP6 climate model.
- 15 • Stratospheric mean ages are significantly improved compared to the lower verti-  
16 cal resolution version of ModelE.
- 17 • The stratospheric transport response to increased CO<sub>2</sub> is approximately linear and  
18 correlated with the magnitude of surface warming.

## Abstract

Here we examine the large-scale transport characteristics of the new “Middle Atmosphere” NASA Goddard Institute for Space Studies climate model (E2.2). First we evaluate the stratospheric transport circulation in historical atmosphere-only simulations integrated with interactive trace gas and aerosol chemistry. Compared to lower vertical resolution model versions, E2.2 exhibits improved tropical ascent and older stratospheric mean ages that are more consistent with observed values. In the troposphere, poleward transport to the Arctic and interhemispheric mean ages in E2.2 are comparable to models participating in the Chemistry Climate Modeling Initiative.

In addition to validating E2.2 we also assess its “transport sensitivity” using the coupled atmosphere-ocean abrupt  $4\times\text{CO}_2$  and transient  $1\%\text{CO}_2$  simulations submitted to the Coupled Model Intercomparison Project, Phase 6, along with a  $2\times\text{CO}_2$  simulation used to evaluate the linearity of the transport circulation’s response to increased  $\text{CO}_2$ . We show that decreases (increases) in a stratospheric mean age (idealized surface loss) tracer scale linearly with increased lower stratospheric upwelling, which also increases linearly with warming tropical sea surface temperatures (SSTs). Abrupt  $2\times\text{CO}_2$  and  $4\times\text{CO}_2$  experiments constrained with (fixed) pre-industrial SSTs are also used to quantify the relative importance of rapid adjustments versus SST feedbacks to the transport circulation responses in the model. Finally, sensitivity experiments are presented to illustrate the impact of changes in the convective parameterization on stratospheric transport.

## 1 Introduction

It is now well appreciated that the stratosphere plays an important role in shaping the chemical, dynamical and radiative properties at Earth’s surface on a range of timescales. On climatic timescales these include the modulation of the Southern Hemisphere midlatitude jet and Southern Ocean ventilation changes by stratospheric ozone depletion (e.g., Polvani et al. (2011); Waugh et al. (2013)). On seasonal timescales, the stratosphere also influences surface weather over both the extra-tropics (e.g. Gerber et al. (2012); Scaife et al. (2016); Seviour et al. (2014)) and in the tropics (Yoo & Son, 2016). While some of these influences are almost exclusively dynamical in nature, others are largely mediated by atmospheric composition, most notably through changes in stratospheric ozone, which influences lower stratospheric temperature gradients and, via thermal wind balance, the tropospheric midlatitude jet streams. Therefore, in order to capture the full effect of the stratosphere on surface climate trends and variability it is important that models properly simulate stratospheric composition including, but not limited to, ozone, water vapor, and stratospheric aerosols.

The global-scale characteristics of stratospheric tracers (and their mutual relationships) are dominated not only by mean diabatic advection (upwelling in the tropics, downwelling in the surf zone and the vortex) but also by rapid isentropic stirring within the surf zone (Plumb, 2002). Therefore, in order to properly simulate stratospheric composition it is important that models not only accurately represent dynamical measures like the residual mean (or Transformed Eulerian Mean) circulation (D. G. Andrews et al., 1987) but, also, the integrated effects of advection and isentropic mixing, as captured through “tracer-independent” measures of the transport circulation (Holzer & Hall, 2000) like the stratospheric mean age (Hall & Plumb, 1994).

In Part I of this study Rind et al. (2020) (hereafter R20) presented a comprehensive overview of the new NASA Goddard Institute for Space Studies (GISS) Middle Atmosphere (MA) Model E2.2. While that study examined a range of key dynamical features of E2.2, both with respect to its mean state (e.g. Hadley Cell strength, zonal winds) as well as its variability (e.g. Madden-Julian Oscillation, the Quasi-Biennial Oscillation (QBO), Stratospheric Sudden Warmings), here we present an overview of the large-scale

transport characteristics of the model. As in that study we focus primarily on the stratosphere, which differs most compared to the lower vertical resolution version of GISS ModelE (E2.1) (Kelley et al., 2019) with which we compare directly in addition to comparing against observations. In particular, the stratospheric transport circulation in E2.2 is expected to reflect not only the large-scale (largely advective) dynamical features discussed in Part I, but also the representation of isentropic mixing within the middle and lower stratosphere, which is sensitive to vertical resolution as it depends on how well meridional and vertical tracer gradients are represented.

For sake of brevity we focus our evaluation of E2.2 around the atmosphere-only (AMIP) historical and coupled atmosphere-ocean increased carbon dioxide (CO<sub>2</sub>) simulations that have been submitted as part of the DECK to the Coupled Model Intercomparison Project, Phase 6 (CMIP6) (Eyring et al., 2016), using the former to validate the model’s large-scale transport characteristics and the latter to evaluate the climate response of the transport circulation. Although not requested for any particular “MIP”, all simulations presented here were integrated carrying a range of idealized tracers that provide canonical measures for evaluating large-scale transport as used in previous (non-CMIP) intercomparisons of chemistry climate models, including the Stratospheric Processes and their Role in Climate (SPARC) CCMVal (CCMVal, 2010) and, more recently, the Chemistry-Climate Model Initiative (CCMI) (Eyring et al., 2013).

Our discussion of the climate change response in the stratospheric and tropospheric transport circulations is in the context of the abrupt CO<sub>2</sub> forcing simulations which, despite their simplicity, afford a mechanistic look into the response characteristics of models that can be unambiguously attributed to an increase in CO<sub>2</sub> concentrations. This simple forcing lens is especially important for understanding the large-scale transport response to climate change, which has been relatively unexplored in previous studies that have either focused almost exclusively on “dynamical sensitivity” (Grise & Polvani, 2016; Chemke & Polvani, 2019; Menzel et al., 2019) or on the large-scale transport circulation response to changes in both CO<sub>2</sub> (and other greenhouse gases (GHGs)) and ozone depleting substances (ODS) (Doherty et al., 2017; Abalos et al., 2019). The CO<sub>2</sub>-induced response of the large-scale transport circulation therefore remains poorly understood.

We begin by comparing in Section 3 various chemical and transport measures in the CMIP6 historical simulations of E2.2 over the recent satellite period with observations, when available. In those cases where comparisons with observations are not possible we compare E2.2 directly with results from the CCMI models presented in Orbe et al. (2019) in an effort to place Model E2.2 in the broader context of similar high vertical resolution chemistry climate models (CCMs). Then we present different measures of “transport sensitivity” in E2.2 in Section 4 along with a discussion of the sensitivity of different aspects of the stratospheric transport circulation to changes in (parameterized) convection and how this informed model development (Section 5). Conclusions are then presented in Section 6.

## 2 Analysis Approach

Here we review the models, simulations and transport and chemical measures used in our analysis. The observational products against which the simulations are compared are also discussed.

### 2.1 Models: E2.2(-AP) and E2.1

Our analysis focuses on the NASA GISS “Middle Atmosphere” model E2.2, which was documented extensively in R20 in terms of its key radiative and dynamical properties. Unlike previous MA versions of ModelE, E2.2 has contributed to CMIP6, with all DECK simulations having thus far been submitted to the Earth System Grid Fed-

eration (<https://esgf.lln1.gov>), for the case of the coupled atmosphere-ocean model utilizing non-interactive (NINT) chemistry. Interactive versions of the E2.2 DECK are currently processing and will also be made available upon their completion.

As described in R20, E2.2 consists of 102 vertical levels spanning the surface up to 0.002 hPa, as compared to the lower vertical resolution of ModelE (E2.1), which consists of 40 levels extending up to 0.1 hPa. Orographic and non-orographic gravity wave drag (GWD) is parameterized following Lindzen (1984) and Rind et al. (1988), producing in E2.2 a Quasi-Biennial Oscillation that compares well with observations as well as improved stratospheric polar vortex variability (R20, Ayarzagüena et al. (2020)). We refer the reader to R20 for an in-depth discussion of the model.

Among the different model versions discussed in R20 here we focus on the “Altered-Physics” (-AP) version E2.2-AP because this is the configuration that was submitted to CMIP6 and presented in Ayarzagüena et al. (2020). While this version does differ from the “standard” model version E2.2 in certain respects (i.e. convective mass flux profiles, high cloud cover, planetary albedo, shortwave absorbed at the surface) the climatologies of both model versions agree overall quite well, especially with respect to their stratospheric transport properties, as discussed in Sections 3 and 4.

Finally, R20 reviewed aspects of the dynamical parameterizations that differ between E2.1 and E2.2, including, among others, incorporation—and subsequent tuning—of an “efficiency factor” relating convection to parameterized gravity wave momentum fluxes (see R20 for more). In addition, while the gas phase chemistry formulation in E2.2 is that used in E2.1, changes in the dynamics and thermodynamic structure associated with the higher model top in E2.2 necessitated a re-tuning of some aspects of the photolysis code. In particular, in E2.1 overhead ozone above the top of the chemistry is taken to be constant, whereas in E2.2 it is given a spatial variation to match that of ozone at the top layer of chemistry. In addition, certain photolysis rates tunings at short wavelengths ( $< 200$  nm) for  $\text{N}_2\text{O}$  and  $\text{O}_2$ , which in E2.1 corrected for stratospheric circulation-induced biases in high latitude  $\text{NO}_x$  and  $\text{O}_3$ , were disabled in E2.2.

## 2.2 Experiments

### 2.2.1 E2.2-AP CMIP6 DECK Simulations

The bulk of our analysis presents results from the CMIP6 DECK experiments performed using E2.2-AP. For purposes of validating the model we begin by first discussing the results from the AMIP historical simulations constrained with observed sea surface temperatures (SSTs) and prescribed sea ice concentrations (SICs) (Table 1, rows 1-2). Specifically, we utilize the “OMA” (AMIP) version of E2.2-AP described in R20 in which aerosols and trace gases are calculated interactively using the OMA (“one-moment aerosol”) scheme (“TCADI” in CMIP5). Results from three members of the E2.2-AP ensemble are presented (row 1). In addition, one member of a 5-member E2.2 OMA AMIP ensemble is also presented (row 2) in order to show that the “Altered Physics” version of the model exhibits quite similar stratospheric transport characteristics to those of the “standard” E2.2 version. Note that we only use one member for the latter since the transport differences among the three E2.2-AP members is found to be quite small, as demonstrated in Section 3.

After using the AMIP OMA E2.2-AP simulations for validation against the observations, we then present an analysis of the “transport sensitivity” of the “Coupled” model from R20, using results from the E2.2-AP DECK coupled atmosphere-ocean non-interactive pre-industrial control and abrupt and transient  $\text{CO}_2$  simulations (Table 1, rows 4-7). For each simulation only one ensemble member was run for CMIP6 (and shown herein). In particular, we examine the Pre-Industrial (PI) control and “branching” abrupt  $2\times\text{CO}_2$  and  $4\times\text{CO}_2$  and transient  $1\%\text{CO}_2$  experiments. In this study we focus only on runs cou-

168 pled to the GISS Ocean v1 (GO1) (i.e. “-G” in CMIP6 notation, “-R” in CMIP5). Al-  
 169 though E2.2-AP DECK simulations were also performed using the HYCOM dynamical  
 170 ocean (i.e. E2.2-H) they did not integrate the passive tracers that underlie the bulk of  
 171 our analysis and so only E2.2-AP-G results are presented here. Finally, abrupt 2xCO<sub>2</sub>  
 172 and 4xCO<sub>2</sub> experiments constrained with (fixed) pre-industrial SSTs (FIXSST) are also  
 173 used to quantify the relative importance of rapid adjustments versus SST feedbacks (Ta-  
 174 ble 1, rows 8-9).

### 175 **2.2.2 E2.1 CMIP6 Historical Simulation**

176 In addition to validating E2.2 against observations we also compare with the re-  
 177 sults from two members of the E2.1 historical AMIP ensemble presented in R20 that was  
 178 also submitted to CMIP6 (Table 1, row 3). That simulation, which uses the same OMA  
 179 chemical mechanism, is identical to that presented in Kelley et al. (2019) with the ex-  
 180 ception that additional idealized tracer diagnostics were integrated in order to facilitate  
 181 transport comparisons with E2.2. Note that these tracers, as described in Section 2c, are  
 182 passive and do not interact with the model’s physics and/or dynamics.

### 183 **2.2.3 E2.2 Sensitivity Experiments**

184 Unlike some earlier iterations of the MA version of ModelE (i.e. Model III discussed  
 185 in Rind et al. (2014)), E2.2 employs the same underlying physics as in E2.1. There are  
 186 important departures, however. In particular, while both versions use the same deep con-  
 187 vection parameterization (Del Genio et al., 2007), with updates in both models designed  
 188 to enhance the simulation of the MJO (Kim et al., 2013; Kelley et al., 2019), some ad-  
 189 ditional modifications related to how condensate evaporation in convective updrafts in-  
 190 teracts with the wider, non-convecting part of the GCM grid box were incorporated in  
 191 E2.2 and not in E2.1 (R20). The implications of that parameter choice were discussed  
 192 in R20 and will not be presented here as they do not bear immediate relevance to strato-  
 193 spheric transport.

194 By comparison, the other main set of changes to the convective parameterization  
 195 – those that distinguish the “standard” versus “AP” versions of E2.2 – will be briefly  
 196 presented in Section 5 as the experiments that were conducted in the process of devel-  
 197 oping E2.2-AP illustrate how convection changes can affect the stratospheric transport  
 198 characteristics of the model. In deciding on the final version of E2.2-AP we carried out  
 199 several sensitivity experiments utilizing both AMIP and coupled atmosphere-ocean con-  
 200 figurations, only a subset of which is presented here (Table 1, rows 10-11). Our moti-  
 201 vation for presenting these results is not to make any direct inferences about specific as-  
 202 pects of the convective parameterization (which likely will be model dependent) but, rather,  
 203 to illustrate interesting relationships between convection and stratospheric transport that  
 204 we observed in the process of developing E2.2-AP that might be more generally appli-  
 205 cable to other models.

### 206 **2.2.4 Chemistry Climate Modeling Initiative (CCMI) Simulations**

207 Finally, in order to place the E2.2 OMA (AMIP) results in the broader context of  
 208 similar high-top stratosphere-resolving models we compare with the transport evalua-  
 209 tions for the CCMI models presented in Orbe et al. (2019). Specifically, we compare  
 210 against the results from the REF-C1 free-running experiments spanning 1979-2010 which  
 211 were constrained with observed SSTs and SICs and which integrated a broad set of ide-  
 212 alized passive tracers, later implemented in E2.2 as described next.

### 2.3 Chemical and Transport Measures

To evaluate stratospheric transport in E2.2 we use a combination of both real (i.e. methane (CH<sub>4</sub>), nitrous oxide (N<sub>2</sub>O), water vapor (H<sub>2</sub>O) and ozone (O<sub>3</sub>)) and idealized tracers, including the stratospheric mean age of air ( $\Gamma_{\text{STRAT}}$ ) and an annually periodic oscillating tracer ( $\chi_{\text{tape}}$ ) (Hall et al., 1999; Orbe et al., 2017) (Table 2). The latter is used to evaluate tropical ascent and is implemented by prescribing a sinusoid in mixing ratio over 10°S-10°N at 100 mb that has a maximum during October, consistent with the seasonality of water vapor-based estimates of the tape recorder at the tropical tropopause (Mote et al., 1996) and consistent with the implementation in Orbe et al. (2017). At the same time, the mean age provides an integrated measure of the time since air was last at the tropical tropopause. Though not “tracer-independent” (Holzer & Hall, 2000), as is the case for  $\Gamma_{\text{STRAT}}$ , the gradients of CH<sub>4</sub> and N<sub>2</sub>O also provide information about the relative importance of ascent versus in-mixing within the tropical pipe and are common measures for assessing stratospheric transport in models (Eyring et al. (2006)).

In addition to the stratospheric mean age we also investigate transport from the stratosphere to the troposphere through analysis of the residence time of (simulated) bomb-produced <sup>14</sup>C (Prather & Remsberg, 1993; Rind et al., 1999). The initial conditions for the release are taken from Johnston (1989) for the year October 1963, with input peaking at around 20 km at northern mid-latitudes. The lower boundary is varied as in the following prescription (see also Prather and Remsberg (1993)):

$$\chi_{14\text{C}}(\mathbf{r}, t) = \begin{cases} 73.0 - 0.27823t - 3.45648e^{-3t^2} + 4.21159e^{-5t^3} & \text{over the NH} \\ 44.5 + 1.02535t - 2.13565e^{-2t^2} + 8.61853e^{-5t^3} & \text{over the SH} \end{cases}$$

where  $t$  refers to the number of months after October 1963, the units are 10<sup>5</sup> molecules <sup>14</sup>C g<sup>-1</sup> of air and NH and SH refer to the Northern and Southern hemispheres, respectively.

Even for cases when the stratospheric mean age and mean residence time are defined with respect to the same stratospheric entry boundary condition (i.e. the tropical tropopause), the two timescales capture physically distinct aspects of stratospheric transport, with the mean age referring to the population of fluid elements that exits the stratosphere, whereas the residence time characterizes the fluid elements that reside in the stratosphere (Holzer et al., 2012). Hall and Waugh (2000) found that they are correlated, but imperfectly so, particularly for the case of release sources occurring in the mid-latitude lower stratosphere, for which variations in the mid-latitude tropopause height strongly affect the residence time but not the mean age.

After analyzing stratospheric transport we then use a combination of other idealized tracers to evaluate different aspects of large-scale tropospheric transport. In order to place E2.2 in the broader context of other CCMs we use tracers that were also implemented in the CCM1 REF-C1 integrations and evaluated in Orbe et al. (2019). In particular, we examine two idealized loss tracers that are emitted over the Northern Hemisphere (NH) midlatitude surface (30°N-50°N),  $\chi_{\text{NH},5}$  and  $\chi_{\text{NH},50}$ , and decay uniformly with loss frequencies of 5 days<sup>-1</sup> and 50 days<sup>-1</sup>, respectively.

In addition, we consider a tropospheric mean age tracer  $\Gamma_{\text{NHMID}}$  (not to be confused with  $\Gamma_{\text{STRAT}}$ ) that describes the mean time since air was at the NH midlatitude surface. Unlike other measures of interhemispheric transport, the mean age can be calculated for locations throughout the troposphere and thus provides more information on transport times than the interhemispheric exchange time (Geller et al., 1997; Levin & Hesshaimer, 1996), which only quantifies the transport between hemispheres (Waugh et al., 2013). In order to facilitate comparisons of simulated values of  $\Gamma_{\text{NHMID}}$  with observations we also integrate a sulfur hexafluoride (SF<sub>6</sub>) tracer using the same power grid source distribution implemented in Rind et al. (1999) and subject to increases of 0.3 pptv/year.

261 From SF<sub>6</sub> we then define an SF<sub>6</sub> age ( $a_{SF6}$ ) as the time lag satisfying

$$\chi(\mathbf{r}, t) = \chi_0(t - a_{SF6}) \quad (1)$$

262 where  $\chi(\mathbf{r}, t)$  refers to the SF<sub>6</sub> concentration at a location  $\mathbf{r}$  and field time  $t$  and  $\chi_0$  refers  
 263 to the concentration of SF<sub>6</sub> over the source region (here, the NH midlatitude surface).  
 264 Note that, unlike for the case of the  $\Gamma_{NHMID}$  tracer, which was implemented identically  
 265 as in the CCMi models, the emissions for the SF<sub>6</sub> tracer in ModelE are different than  
 266 the more recent emissions distributions used in CCMi, which were taken from EDGAR  
 267 v4.2 (Yang et al., 2019). Therefore, while the tropospheric mean age tracer ( $\Gamma_{NHMID}$ )  
 268 is used to compare E2.2(-AP) and E2.1 with the CCMi models, the SF<sub>6</sub> age tracer is used  
 269 for comparing against observations.

270 While we use  $\Gamma_{NHMID}$  and  $a_{SF6}$  as integrated measures of interhemispheric trans-  
 271 port, we also examine subtropical convection through use of a radon tracer (Rn-222),  
 272 the vertical distribution of which is governed primarily by fast local mixing processes,  
 273 owing to its surface source derived from the decay of uranium ore (U-238) in soils and  
 274 its half-life of 3.8 days. Unfortunately, very few observed vertical profiles exist in the trop-  
 275 ics or subtropics for comparisons with models. Therefore, our evaluations of simulated  
 276 radon in the subtropics are limited to profiles at only one location (Rani et al., 2014),  
 277 as discussed in Section 3. Additional comparisons of Rn-222 with the observed profiles  
 278 over northern midlatitudes from Murray et al. (2014) are also performed.

279 Finally, we consider the distribution of the idealized tracer “e90” to quantify trans-  
 280 port in the upper troposphere/lower stratosphere (UTLS), with regards to both its in-  
 281 terannual variability (Abalos et al., 2017) as well as its response to climate change (Abalos  
 282 et al., 2019). Specifically, e90 is emitted at the Earth’s surface and decays uniformly with  
 283 a lifetime of 90 days<sup>-1</sup> throughout the atmosphere.

## 284 2.4 Observational Products

285 Various observational products are used to evaluate the chemical and transport char-  
 286 acteristics of the E2.2 historical simulations (Table 2, col. 3). Several of these were used  
 287 in CCMVal (2010), and are included here to ensure consistency in our (stratospheric)  
 288 transport evaluation with that of other models, except in cases where new observations  
 289 correct for known biases in the older products.

290 In particular, the simulated fields of CH<sub>4</sub>, O<sub>3</sub> and H<sub>2</sub>O are compared with the cli-  
 291 matologies derived for 1991-2002 from the Halogen Occultation Experiment (HALOE)  
 292 on board the Upper Atmosphere Research Satellite (UARS) (Groß & Russell, 2005).  
 293 Comparisons of simulated N<sub>2</sub>O are made against 2005-2015 climatologies derived from  
 294 the Microwave Limb Sounder (MLS) on the Earth Observing System (EOS) Aura satel-  
 295 lite. We use the 190-GHz retrieval from version 4.2 because the 640-GHz data set ends  
 296 in summer 2013 due to the failure of the N<sub>2</sub>O primary band. Note that any recent lower  
 297 stratospheric changes in N<sub>2</sub>O (those occurring after 2015) are not considered in this study  
 298 (Personal Communication with Krzysztof Wargan). For ozone, in addition to the strato-  
 299 spheric profiles from HALOE, total column ozone fields are also evaluated against the  
 300 Total Ozone Mapping Spectrometer (TOMS) and the Ozone Monitoring Instrument (OMI)  
 301 (TOMS for years 2000-2004 and OMI for 2005-2010) (R. McPeters et al., 2008). Histor-  
 302 ical trends in simulated total column ozone (TCO) are compared against the ground-  
 303 based measurements based on the Dobson and Brewer spectrophotometer and filter ozonome-  
 304 ter observations available from the World Ozone and UV Data Centre (WOUDC) up-  
 305 dated from (Fioletov et al., 2002). In addition to the ground-based observations, which  
 306 date back to 1964, we also compare simulated TCO values to the monthly mean zonally  
 307 averaged SBUV (Version 8.6) merged ozone dataset extending back to January 1970  
 308 (R. D. McPeters et al., 2013).

309 In addition to our evaluations of the chemical tracers, simulated values of the strato-  
 310 spheric mean age ( $\Gamma_{\text{STRAT}}$ ) are compared first against meridional age profiles derived  
 311 from in-situ aircraft measurements of carbon dioxide ( $\text{CO}_2$ ), averaged in  $2.5^\circ$  latitude  
 312 bins over the altitude range 19.5-21.5 km (Boering et al. (1996), see also Figure 5 in Hall  
 313 et al. (1999)). Vertical profiles of simulated  $\Gamma_{\text{STRAT}}$  are also compared in the tropics against  
 314 the average of in situ-based estimates derived separately from  $\text{CO}_2$  and  $\text{SF}_6$  sampled over  
 315  $10^\circ\text{S}$ - $10^\circ\text{N}$  between 15.2-34.2 km and 15.2-34 km, respectively. Over midlatitudes only  
 316 the  $\text{CO}_2$ -based age profiles are used, which apply to latitudes spanning  $34^\circ\text{N}$ - $44^\circ\text{N}$  and  
 317 altitudes between 11.1 and 35.1 km (A. E. Andrews et al., 2001; Engel et al., 2009). HALOE  
 318  $\text{H}_2\text{O}$  fields are used to obtain the observational-based tape recorder ( $\chi_{\text{tape}}$ ) phase lag val-  
 319 ues presented in this study and mirror those shown in Hall et al. (1999) (See their Fig-  
 320 ure 16).

321 Finally, simulated values of the  $\text{SF}_6$  age ( $a_{\text{SF}_6}$ ) are compared against the observed  
 322 profiles that were presented in Waugh et al. (2013) (see their Figure 3). In the calcula-  
 323 tion of  $a_{\text{SF}_6}$  from the observations,  $\chi_0$  (from Equation 1) is taken to be the average of  
 324  $\text{SF}_6$  obtained from surface flask measurements from three NH midlatitude stations (Mace  
 325 Head ( $53.5^\circ\text{N}$ ), Niwot Ridge ( $40^\circ\text{N}$ ) and THD (Trinidad Head,  $41^\circ\text{N}$ )) from the NOAA  
 326 Halocarbons and other Atmospheric Trace Species (HATS) group. The  $\text{SF}_6$  age at south-  
 327 ern latitudes is then calculated using a combination of measurements from both ground  
 328 stations, including HATS as well as the discrete air samples collected from the NOAA  
 329 Carbon Cycle Greenhouses Gases (CCGG) group, and commercial ships. We refer the  
 330 reader to Waugh et al. (2013) for more details.

### 331 3 Transport Evaluation of E2.2 CMIP6 Historical AMIP Simulations

332 We begin by presenting climatologies of various stratospheric constituents that can  
 333 be directly compared with observations and, in turn, provide an indirect measure of how  
 334 well the transport circulation is being simulated in the model. We then present a com-  
 335 parison of the tracer-independent measures of transport (i.e. both stratospheric and tropo-  
 336 spheric mean ages, the tape-recorder phase lag) for which some observational constraints  
 337 are available and, in cases where they are not, comparisons are made directly with the  
 338 CCM1 models.

#### 339 3.1 Stratospheric Transport Circulation

##### 340 3.1.1 Annual Climatological Stratospheric $\text{CH}_4$ , $\text{N}_2\text{O}$ , $\text{O}_3$ and $\text{H}_2\text{O}$

341 Zonal mean comparisons of methane ( $\text{CH}_4$ ) between E2.2-AP and HALOE (Fig.  
 342 1a (top), Supplementary Fig. 1a (top)) show good agreement throughout the lowermost  
 343 stratosphere (30-100 hPa) over both the tropics and extra-tropics, in terms of both mean  
 344 values in the tropics and in terms of the meridional slopes of tracer isopleths over the  
 345 subtropics and midlatitudes. (Note that only latitudes between  $60^\circ\text{S}$ - $60^\circ\text{N}$  are shown for  
 346 HALOE, owing to uncertainties in the measurements over the poles, which vary with sea-  
 347 son (see Grooß and Russell (2005) for more). Overall, the absolute values and, in par-  
 348 ticular, isopleth shapes over the extra-tropics in E2.2-AP are improved compared to in  
 349 E2.1 (Fig. 1a, bottom), although their gradients are still somewhat weaker compared to  
 350 the observations. In E2.1 the presence of much weaker gradients in the subtropics and  
 351 midlatitudes in both hemispheres is indicative of a leakier tropical pipe. This excessive  
 352 leakiness in E2.1 is consistent with much larger transient eddy kinetic energy biases in  
 353 that model throughout the subtropical middle and lower stratosphere, as compared to  
 354 E2.2-AP (not shown).

355 Stronger meridional gradients in the lower stratosphere in E2.2-AP are also exhib-  
 356 ited in other tracers, including  $\text{N}_2\text{O}$  (Fig. 1b, Supplementary Fig. 1b). In addition to  
 357 improved gradients, the absolute values of  $\text{N}_2\text{O}$  in E2.2-AP also exhibit overall much bet-



358 ter agreement with the observations, compared to E2.1. One exception, however, is the  
 359 tropical middle stratosphere ( $\sim 10\text{-}20$  hPa) where E2.2-AP exhibits a low ( $\sim 10\%$ ) bias  
 360 (featured also in methane), that is not seen in E2.1, which exhibits values at 20 hPa  
 361 ( $24 \times 10^{-8}$  V/V) that compare well with MLS. As discussed in the next section, these lo-  
 362 calized tropical mid-stratospheric biases in E2.2-AP most likely reflect excessive in-mixing  
 363 between the tropics and subtropics in that region.

364 Moving next to ozone, we find that  $\text{O}_3$  concentrations in both E2.1 and E2.2-AP  
 365 compare well with observed values over all latitudes and for pressures greater than 30  
 366 hPa (Fig. 1c, Supplementary Fig. 1c). In the lowermost stratosphere (i.e. 50-100 hPa)  
 367 the ozone concentrations in both models are similar, albeit smaller in E2.2-AP poleward  
 368 of  $40^\circ\text{S/N}$  and larger in the tropics and subtropics. The smaller stratospheric ozone val-  
 369 ues in E2.2-AP over latitudes poleward of  $40^\circ\text{S/N}$  most likely contribute to the overall  
 370 smaller total ozone burdens in that model, compared to E2.1, manifest both in the seasonal  
 371 cycle and historical trends as discussed in Sections 3.3 and 3.5, respectively.

372 Above 30 hPa, the ozone values in E2.2-AP are too low in the tropics, a bias also  
 373 exhibited in E2.2 (not shown). One way to interpret this low bias, which is not exhib-  
 374 ited in E2.1, is in terms of greater tropical upwelling in this region in E2.1 compared to  
 375 E2.2(-AP), which is manifest in stratospheric mean age differences between the models  
 376 (Fig. 2) as discussed more in the next section. However, while this explains the  $\text{O}_3$  dif-  
 377 ferences between E2.2(-AP) and E2.1, it does not explain why E2.2(-AP) is biased low,  
 378 compared to the observations. Moreover, the fact that this (relatively localized) ozone  
 379 bias also occurs in a region of low  $\text{CH}_4$  and  $\text{N}_2\text{O}$ , indicates that it is also likely not fun-  
 380 damentally driven by photolysis differences between the models but, rather, more likely  
 381 reflects a more general dynamical circulation bias in E2.2.

382 To this end, further inspection of the zonal winds in this region (Figures 5 and 35  
 383 in R20) reveals a localized region of anomalous westerlies in both E2.2-AP and E2.2 not  
 384 present in E2.1 during boreal winter. Compared to the overall climatological wind and  
 385 temperature distributions in the stratosphere, which are much improved in E2.2(-AP)  
 386 compared to E2.1 (R20), this bias is small in amplitude and regional in nature. Nonethe-  
 387 less, its presence may have an impact on the transport properties in that region. In par-  
 388 ticular, while their origins are not well understood, in addition to having a direct advective  
 389 impact on tracer transport in the tropics, these localized wind biases are also asso-  
 390 ciated with changes in meridional potential vorticity (PV) gradients which can directly  
 391 impact mixing into and out of the tropical pipe. Indeed, as shown in Eichinger et al. (2020),  
 392 the incorporation of non-orographic gravity wave drag in simulations using the EMAC  
 393 chemistry climate model has a significant impact on the strength of PV gradients (and  
 394 associated mixing) in this region (i.e. the tropics spanning pressures between 2-20 hPa)  
 395 (See their Figure 8). Therefore, the incorporation of additional non-orographic GWD  
 396 sources in E2.2(-AP) may also impact tropical transport indirectly through changes in  
 397 mixing, not only through the direct (advective) changes associated with explicit simu-  
 398 lation of the QBO, as discussed later.

399 Finally, comparisons of stratospheric water vapor show good agreement between  
 400 E2.2-AP and HALOE, albeit with a slightly low bias ( $\sim 5\%$ ) over the northern midlat-  
 401 itude stratosphere and a wet bias ( $\sim 5\%$ ) over the tropical lower stratosphere (Fig. 1d,  
 402 Supplementary Fig. 1d). The water vapor fields in E2.2-AP represent an improvement  
 403 over E2.1 in terms of both absolute magnitudes (E2.1 is biased low by  $\sim 10\text{-}20\%$ ), as well  
 404 as in terms of meridional gradients over the extra-tropical stratosphere. The larger val-  
 405 ues in E2.2-AP in the tropical lower stratosphere are most likely associated with a warmer  
 406 tropical tropopause cold point temperature, which is warmer by  $\sim 1\text{-}2$  degrees in E2.2-  
 407 AP, compared to E2.1, which is biased cold (see Figure 4 in R20 which also shows that  
 408 E2.2-AP is biased  $\sim 0.5\text{-}1.0$  degrees warm relative to reanalysis fields). Furthermore, we  
 409 note that E2.2, which is still warmer in the tropopause region, exhibits a slightly wet-  
 410 ter bias (not shown). Thus, while details of the processes that control stratospheric wa-

411 ter vapor remain controversial (Danielsen, 1993; Sherwood & Dessler, 2000; Holton &  
 412 Gettelman, 2001), the lower tropical stratospheric biases in the different versions of Mod-  
 413 elE do seem to be very much tethered to their respective climatological cold point tem-  
 414 peratures, consistent with previous studies (Randel et al., 2004).

### 415 *3.1.2 Annual Climatological Mean Age, $^{14}\text{C}$ Residence Time and “Tape 416 Recorder” Tracers*

417 The previous section provides only indirect evidence that aspects of the stratospheric  
 418 transport circulation have improved in E2.2. Here we explicitly examine the transport  
 419 circulation through comparisons of the stratospheric mean age ( $\Gamma_{\text{STRAT}}$ ) and tropical  
 420 ascent phase estimates inferred from the idealized tape recorder tracer ( $\chi_{\text{tape}}$ ). Given  
 421 that neither the mean age nor tape-recorder tracers are directly observable, we compare  
 422 the ModelE results with both in-situ based approximations (derived from  $\text{SF}_6$ ,  $\text{CO}_2$  and  
 423  $\text{H}_2\text{O}$ ) as well as the CCMI simulated fields.

424 We begin with the mean age (Fig. 2a,b),  $\Gamma_{\text{STRAT}}$ , which features characteristic iso-  
 425 leths that ascend in the tropics and slope down over higher latitudes in both hemispheres  
 426 with values in E2.2-AP (E2.1) corresponding to  $\sim 1$  (0.5) year(s) in the tropical lower  
 427 stratosphere and  $\sim 5$  (3.5) years over polar latitudes in the middle stratosphere. Direct  
 428 comparisons of  $\Gamma_{\text{STRAT}}$  at 20 km (Fig. 3a) as well as over the tropics (Fig. 3b) and north-  
 429 ern midlatitudes (Fig. 3c) show very good agreement between E2.2-AP and observational  
 430 estimates, as well as with the CCMI models. (Note that the differences between the three  
 431 individual ensemble members is very small). While the ages in E2.2 are slightly (5%) younger  
 432 than in E2.2-AP, those differences are negligible compared to the differences relative to  
 433 E2.1, for which the mean age values are  $\sim 30\%$  too young, consistent with the values re-  
 434 ported for previous versions of the lower vertical resolution version of ModelE (Shindell  
 435 et al., 2013).

436 In addition to the mean age, Fig. 3d shows changes in the stratospheric concen-  
 437 tration of  $^{14}\text{C}$  as a function of month after release in the mid-stratosphere, compared among  
 438 E2.2-AP, E2.2 and E2.1. Results are presented using natural log coordinates, and also  
 439 shown are the stratospheric residence time,  $\tau_{^{14}\text{C}}$  (the inverse of the associated least mean  
 440 squares slope). While it is well known that  $\tau_{^{14}\text{C}}$  evolves as a function of time after the  
 441 pulse is released (consistent with changes in the stratospheric distribution of that tracer)  
 442 for sake of brevity we consider here only residence times after 100 months, for which  $\tau_{^{14}\text{C}}$   
 443 corresponds to 4.76, 4.63 and 4.21 years for E2.2-AP, E2.2 and E2.1 respectively. Com-  
 444 parisons with the observed values presented in Prather and Remsberg (1993) indicate  
 445 that, overall, the greater stratospheric residence times in E2.2(-AP) are more consistent  
 446 with observations for this particular radionuclide, a result that complements the mean  
 447 age assessment presented earlier. Further comparisons of the spatial distribution of  $^{14}\text{C}$   
 448 (not shown) also show more coherent cross-tropopause transport in the vicinity of the  
 449 northern subtropical jet in E2.2(-AP), compared to the relatively more noisy pattern ex-  
 450 hibited in E2.1.

451 A similar calculation was made for pre-industrial times, and the residence times  
 452 were about five months longer for the E2.2 models, and 1 month longer in E2.1. This  
 453 suggests that the stratospheric residence time in the more modern time period has de-  
 454 creased, with the effect more noticeable in the E2.2 runs. This might well be associated  
 455 with an increase in the residual circulation due to global warming in the model, an ef-  
 456 fect less evident in E2.1 due to its cruder representation of that circulation.

457 While the mean age and  $^{14}\text{C}$ -based residence time represent integrated measures  
 458 of the effects of both mixing and advection on stratospheric transport timescales, the ver-  
 459 tical propagation of the tape recorder tracer provides a more direct measure of the ad-  
 460 vective transport timescale for ascent to occur within the tropics (Figure 2c,d). In par-  
 461 ticular, we focus on the evolution of  $\chi_{\text{tape}}$  over 5 years at the beginning of the simula-

tions (1980-1985). This is because during the course of the (multi-year-long) simulations the near-tropopause gradients of  $\chi_{\text{tape}}$  weaken substantially, since that tracer is not subject to any stratospheric or tropospheric loss.

Examination of the tape recorder phase lag,  $\phi_{\text{tape}}$  (Fig. 3e), shows good agreement between E2.2(-AP) and observational estimates derived from HALOE water vapor measurements. While ascent is slightly faster in E2.2 compared to E2.2-AP, consistent with the slightly younger mean ages in that model version, this difference is smaller than the differences relative to E2.1, for which the phase lag values are consistently  $\sim 25\%$  too small, compared to the observations. Similar differences in tropical ascent are evident in comparisons of the tape recorder inferred directly from simulated water vapor (Supplementary Figure 3). Note that in Fig. 3e the phase lags from the CCMi models are not shown as they did not integrate the tape-recorder tracer.

Finally, in order to provide a related, but distinct, measure of the strength of in-mixing from the subtropics into the tropical stratosphere, we compare profiles of  $\text{CH}_4$ , averaged over  $10^\circ\text{S}$ - $10^\circ\text{N}$  (Fig. 3f). To ensure consistency with the analysis presented in CCMVal (2010) (see their Figure 5.7) we normalize the climatological tropical mean methane profiles from all models (including the CCMi output) to the HALOE values at the bottom level of the region of interest (100 hPa). All model output is then interpolated to the HALOE vertical levels and then compared directly against the observations. Below 30 hPa the methane vertical gradients exhibited in E2.2(-AP) are in line with the observational estimates and the CCMi models, while the vertical gradients in E2.1 are relatively stronger (Fig. 3f). Above 50 hPa the methane vertical gradients are stronger than those exhibited in the observations (but still within the CCMi intermodel spread), which could be indicative of excessive in-mixing into the tropical middle stratosphere, as alluded to earlier. The region over which this occurs, however, is relatively narrow as it is confined to the tropics spanning 10-30 hPa and may explain some of the negative ozone biases in that region exhibited in E2.2(-AP).

### 3.1.3 Seasonality of Stratospheric $\text{CH}_4$ , $\text{N}_2\text{O}$ , $\text{O}_3$ and $\text{H}_2\text{O}$

Comparisons of the seasonal cycle of  $\text{CH}_4$ ,  $\text{N}_2\text{O}$ , and  $\text{H}_2\text{O}$ , averaged over the middle-to-lower stratosphere (30-100 hPa), also show overall good agreement between E2.2(-AP) and the observations, albeit with some biases depending on the latitude (Fig. 4a-b,d, Supplementary Fig. 2a-b,d). Compared to E2.1, E2.2-AP exhibits stronger meridional gradients in the subtropics along with their seasonal migration, consistent with a stronger subtropical transport barrier in that model. This is especially evident in  $\text{CH}_4$  (Fig. 4a),  $\text{H}_2\text{O}$  (Fig. 4d, Supplementary Fig. 2d) and in  $\text{N}_2\text{O}$  (Fig. 4b, Supplementary Fig. 2b).

The seasonal cycle of total column ozone in E2.2-AP also compares well overall with the TOMS/OMI observations, with maximum values of  $\sim 415$  DU over the NH pole during boreal winter, compared to larger values ( $\sim 450$  DU) in E2.1 (Fig. 4c, Supplementary Fig. 2c). Over the tropics both models exhibit low ozone biases compared to the observations, albeit smaller ones in E2.2-AP (5%) compared to E2.1 ( $\sim 10\%$ ). The smaller low tropical and high polar ozone biases in E2.2-AP are most likely related to a weakening of the Brewer-Dobson circulation, compared to E2.1, as reflected in the older mean ages in that model, with associated weaker transport of ozone-rich air from the tropics to high latitudes. Over the SH high latitudes both E2.1 and E2.2 overestimate observed values during austral winter by about 20-30%, although these biases are slightly smaller in E2.2-AP. While the latter is most likely also associated with an overall weaker circulation in E2.2(-AP) it is also likely that the somewhat improved SH ozone burdens poleward of  $60^\circ\text{S}$  may reflect the improved lower stratospheric temperatures over the SH pole. In particular, the warm austral winter temperature biases in E2.1, which exceed 20 degrees (see Fig. 3c in R20), are reduced to 2-4 degrees in E2.2(-AP) (see Fig. 2b, also in R20).

Finally, it is important to note that the ozone hole in E2.2-AP does not extend quite long enough during September-October-November. Comparisons with the seasonal cycle of H<sub>2</sub>O (Fig. 4d) and CH<sub>4</sub> (Fig. 4a), indicates that this may be driven by an early bias in the seasonality of methane-oxidation driven water vapor production, which may impact heterogeneous ozone depletion on polar stratospheric clouds (PSC).

### 3.1.4 *Interannual Variability Associated with the Quasi-Biennial Oscillation*

One of the key dynamical features introduced in E2.2 that distinguishes it from other GISS models is an accurate interactively generated Quasi-Biennial Oscillation as described in R20. The QBO is a dominant mode of transport variability in the stratosphere that impacts a broad range of trace gases including H<sub>2</sub>O, hydrogen chloride (HCl), O<sub>3</sub>, N<sub>2</sub>O, carbon monoxide (CO), hydrogen fluoride (HF), and CH<sub>4</sub> (Schoeberl et al., 2008; Tweedy et al., 2017), with important implications for the detection of lower stratospheric ozone recovery (Chipperfield et al., 2018), among other applications.

The evolution of the tropical (5°S-5°N) zonal winds for one ensemble member of E2.2-AP (Fig. 5a) compares well with observations (R20) and compared to other CMIP6 models (Orbe et al., 2020), albeit with an amplitude that is about 15% less than observed. (Note that the QBO period difference is negligible between the AMIP configurations of E2.2 (28.5 months) and E2.2-AP (27.7 months) considered here). The imprint of the QBO is manifest in E2.2-AP on a broad range of both chemical and idealized tracers, including methane (Fig. 5b), the stratospheric mean age (Fig. 5c) as well as ozone (Fig. 5d).

In particular, below 10 hPa all species exhibit a clear downward propagation of anomalous negative (positive) values for CH<sub>4</sub> ( $\Gamma_{\text{STRAT}}$ , O<sub>3</sub>) during the westerly shear phase of the QBO, and vice versa. The fact that the anomalies in CH<sub>4</sub> are anti-correlated with those in the mean age and ozone is consistent with the opposite vertical gradients in that tracer (Fig. 1). In particular, during the westerly phase of the QBO the anomalous downwelling associated with warmer anomalies in the tropics draws larger values of  $\Gamma_{\text{STRAT}}$  and O<sub>3</sub> and smaller values of CH<sub>4</sub> into the lower stratosphere. Conversely, easterly wind shear requires colder tropical temperatures and the associated upwelling anomalies bring air from the troposphere into the lower stratosphere, thereby reducing the age of air (and ozone).

While the signature of a QBO extends coherently above 10 hPa to 3 hPa for both methane and the mean age, the ozone anomalies display a more complicated relationship, indicative of a transition between photochemically- versus dynamically-driven regimes (Rind et al., 2014). In particular, above 10 hPa the variability in tropical ozone is shorter and controlled more directly by variations in photolysis; furthermore, in addition to directly affecting the transport of ozone, the warmer temperatures associated with the westerly phase of the QBO at these levels also drive less ozone production. By comparison, below 10 hPa the ozone variations become more clearly modulated by transport associated with QBO dynamics and more closely mirror those of the other tracers. Note that, while the amplitude of the QBO in E2.2 compares well with observations at ~60 hPa (Rind et al., 2020), below 70 hPa the amplitude is weaker than observed, consistent with biases exhibited in other models that produce a QBO (Bushell et al., 2020). In addition to potentially limiting the representation of QBO teleconnections to higher latitudes, this bias also likely affects the amplitude of QBO-driven trace gas variability in the model.

### 3.1.5 *Historical Ozone Changes over 1960-2014*

While the focus of the previous section was on the validation of key stratospheric species with the available satellite measurements, here we consider how the E2.2-G AMIP historical simulations reproduce the evolution of ozone. Figure 6a shows the evolution

of global mean total column ozone in E2.2(-AP) compared with E2.1 and the CCMI models and against both the ground-based measurements from 1960-2014 (Fioletov et al., 2002) and the SBUV v8.6 merged dataset extending back to 1970 (R. D. McPeters et al., 2013). Overall, the total global (90°N-90°S) ozone column decreases over the 1970-1990s are well captured in both models, although the E2.2-AP values are generally smaller than observed; both models also simulate ozone recovery during the years following stratospheric ozone depletion, albeit with lower values. (Note that, while there are some differences in variability during the 1970s, the ground-based and satellite-derived ozone fields agree very well in the global mean). This bias aside, however, the overall performance in both E2.2(-AP) and E2.1 is well within the range of the CCMI models and represents a significant improvement in total column ozone relative to versions of ModelE prior to CMIP5, as discussed in Shindell et al. (2013) and in Kelley et al. (2019).

Comparisons of the Southern Hemisphere (SH) (Fig. 6b) and NH (Fig. 6c) mean total column ozone values also show similar behavior between E2.2(-AP) and E2.1, with somewhat lower values in the former. The overall long-term behavior is similar as well, except that E2.2(-AP) appears to simulate a larger ozone response to the eruption of Mount Pinatubo as well as a faster signature of ozone recovery during the 2000s, which may be linked to the former. In addition, over the Southern Hemisphere there is a distinct discrepancy in the temporal evolution of ozone over the second half of the 1960s between the models. Further inspection of the full historical period (not shown) reveals that these differences in ozone variability are related to differences in the evolution of nitric acid (HNO<sub>3</sub>) following volcanic eruptions, with HNO<sub>3</sub> increasing in E2.2 but decreasing in E2.1. While the response in the former is more consistent with expectations, it is not clear why the models diverge and further work is needed to understand how layer-dependent assumptions made within the code that translate (prescribed) aerosol optical depth to aerosol size may be driving these differences. Finally, there is some indication of larger interannual ozone variability in E2.2-AP over the Northern Hemisphere, relative to E2.1. How (if) this is linked to the more realistic polar vortex variability in that model (R20, Ayarzagüena et al. (2020)) will be examined in future studies.

## 3.2 Tropospheric Transport Circulation

Since the main focus of E2.2 development was towards optimizing the representation of the middle atmosphere, our exposition of the transport characteristics of the troposphere is relatively briefer, compared to the previous section. In addition, there are relatively fewer direct observable constraints on tropospheric transport, owing to the more complex source/sink and emissions distributions of tracers in the troposphere, compared to the stratosphere. Therefore, with the exception of SF<sub>6</sub>, which we use to constrain interhemispheric transport, our focus is primarily on the idealized tracers presented in Orbe et al. (2019) and comparisons with the CCMI models.

### 3.2.1 Transport to the Arctic

The NH midlatitude loss tracers  $\chi_{\text{NH},5}$  (Fig. 7a) and  $\chi_{\text{NH},50}$  (Fig. 7b) show overall good agreement between the ModelE simulated fields over northern midlatitudes and are within the range of the CCMI models, albeit with  $\sim 10\%$  larger values in E2.1, compared to those in E2.2(-AP); by contrast, poleward of 40°N both E2.2(-AP) and E2.1 are biased high, especially for  $\chi_{\text{NH},50}$ . (Note that the E2.2 versus E2.2-AP differences are negligible). While the high bias in  $\chi_{\text{NH},50}$  exhibited in both E2.1 and E2.2 is no larger than  $\sim 10\%$  compared to the CCMI multi-model mean, it is nonetheless consistent with the large carbon monoxide Arctic burdens reported for the CMIP5 version of ModelE by Lee et al. (2013), as compared to models participating in the Atmospheric Chemistry and Climate Model Intercomparison Project (ACCMIP). It is also consistent with the high tropospheric ozone column biases over northern high latitudes noted in Shindell et al. (2013) for previous versions of ModelE (see their Figure 3c). This suggests that this

613 transport bias, which may have implications for black carbon loading over the Arctic (and  
 614 associated radiative forcing), may reflect a systematic, albeit relatively small, bias in the  
 615 model.

616 To explore potential dynamical drivers of the high  $\chi_{\text{NH},50}$  bias over northern polar  
 617 latitudes we perform a seasonal decomposition of  $\chi_{\text{NH},50}$  and find that the higher tracer  
 618 burdens in E2.2(-AP) and E2.1 occur primarily during boreal winter (Supplementary Fig-  
 619 ure 4a,b). Furthermore, comparisons with the climatological mean zonal winds (bottom  
 620 panels) indicates that the biases in  $\chi_{\text{NH},50}$  are associated with biases in the northern mid-  
 621 latitude jet, which is systematically shifted upward in all versions of ModelE, relative  
 622 to the CCMI models (Supplementary Figure 4c). More precisely, as the midlatitude jet  
 623 represents a mixing barrier to along-isentropic poleward transport of surface (high  $\chi_{\text{NH},50}$ )  
 624 tracers, its upward shifted bias would result in more vigorous along-isentropic transport  
 625 to the high latitude upper troposphere (see schematic in Supplementary Figure 5). Note  
 626 that this argument is primarily associated with transport during boreal winter, when along-  
 627 isentropic mixing provides the dominant mechanism for transport from midlatitudes to  
 628 the polar region (Klonecki et al., 2003; Orbe et al., 2013). During other seasons such as  
 629 JJA the mean meridional circulation and across-isentropic transport driven by convec-  
 630 tion become more important (Hess, 2005; Yang et al., 2019).

### 631 **3.2.2 Interhemispheric Transport**

632 We also briefly evaluate simulated interhemispheric transport in terms of the mean  
 633 age since air was last at the NH midlatitude surface,  $\Gamma_{\text{NHMID}}$  (Fig. 7c). The meridional  
 634 profile of  $\Gamma_{\text{NHMID}}$ , as simulated in E2.2(-AP) and E2.1, increases sharply from values of  
 635  $\sim 0.5$  years in the northern tropics to  $\sim 1.8$  years over SH midlatitudes. All ModelE sim-  
 636 ulations (E2.1, E2.2-AP, E2.2) exhibit similar age profiles and fall well within the spread  
 637 spanned by the CCMI models. Furthermore, comparisons with observed  $\text{SF}_6$  age ( $a_{\text{SF}_6}$ )  
 638 profiles (equation (2)), reveals that E2.2 (and E2.1) exhibits mean ages that are older  
 639 than observed, consistent with the CCMI models.

640 To enable a fairer apples-to-apples comparison between  $\Gamma_{\text{NHMID}}$  in the models and  
 641  $a_{\text{SF}_6}$  derived from the observations we also show  $a_{\text{SF}_6}$  for E2.2-AP, as calculated from  
 642 simulated  $\text{SF}_6$  concentrations (cyan line, Fig. 7c). The close correspondence between  $a_{\text{SF}_6}$   
 643 and  $\Gamma_{\text{NHMID}}$  in the SH for E2.2 demonstrates that the mean- and  $\text{SF}_6$ - based ages agree  
 644 well over latitudes far enough away from the (northern midlatitude) source region. (Note  
 645 that we only show  $\Gamma_{\text{NHMID}}$  for the CCMI models as significantly more models integrated  
 646 that tracer, compared to only two models which integrated  $\text{SF}_6$ ). The old age bias in the  
 647 ModelE simulations, manifest in both  $a_{\text{SF}_6}$  and  $\Gamma_{\text{NHMID}}$ , is consistent with a similar bias  
 648 in the CCMI models (Orbe et al., 2019) as well as the TransCom chemistry transport  
 649 (offline) models (Yang et al., 2019). While the latter study posits that the age biases are  
 650 likely driven by biases in transport processes between the northern tropics and extra-  
 651 tropics, a more in-depth examination of the biases in ModelE is beyond the scope of this  
 652 study and is reserved for future work.

### 653 **3.2.3 Upper Troposphere/Lower Stratosphere Transport**

654 As in Abalos et al. (2017) we use the idealized loss tracer e90 to evaluate transport  
 655 in the upper troposphere and lower stratosphere (UTLS). While e90 does not provide  
 656 a direct estimate of the stratosphere-to-troposphere (STT) (or troposphere-to-stratosphere)  
 657 air mass *flux*, versus other measures (Appenzeller et al., 1996; Gettelman & Sobel, 2000;  
 658 Orbe et al., 2012), it correlates well with stratospherically sourced idealized tracers (i.e.  
 659  $\chi_{\text{ST8025}}$  analyzed in Orbe et al. (2019)) and, most importantly, was incorporated in the  
 660 CCMI idealized tracer package, thus providing a means for comparing UTLS transport  
 661 properties of E2.2 with those of other models.

As shown in Fig. 7d there is good agreement in the meridional 100-500 hPa averaged distributions of e90 between E2.1, E2.2-AP and E2.2 and with the CCMI models over the subtropics and tropics. Poleward of 40°S/N, especially in the NH, all versions of ModelE tend to exhibit larger values, compared to the range spanned by CCMI. The e90 biases are consistent in amplitude (and order among the ModelE simulations) with the biases in  $\chi_{\text{NH},50}$ , which is somewhat to be expected given that both tracers have surface sources. However, given its longer lifetime and more global surface source distribution, we also expect that the e90 biases not only reflect potentially excessive transport from the NH midlatitude surface into the northern upper troposphere, but also other transport processes occurring in the lower stratosphere.

In particular, comparisons of the ensemble mean annually and hemispherically averaged climatological cross-tropopause flux over the NH for E2.1 ( $-2.5 \times 10^{-4}$  kg/m<sup>2</sup>/s) compared to E2.2-AP ( $-4.3 \times 10^{-4}$  kg/m<sup>2</sup>/s) (and  $-4.1 \times 10^{-4}$  kg/m<sup>2</sup>/s for E2.2) reveal weaker downward mass transport in E2.1, consistent with less downward exchange of low-e90 stratospheric air masses into the upper troposphere. This suggests that differences in transport from the stratosphere may also be playing a role in the e90 biases over high latitudes. It is important to note that both the cross-tropopause flux and e90 tracer signatures are not merely reflections of circulation differences over high latitudes but also differences in tropopause height among the models, which is biased high over the tropics and northern extra-tropics in E2.1, compared to E2.2(-AP) and the CCMI models (Supplementary Figure 6). Namely, higher mid-to-upper tropospheric burdens of e90 are consistent with a higher tropopause in E2.1; by comparison, both the tropopause and e90 values in E2.2(-AP) are in better agreement with the CCMI models (Fig. 7d), particularly equatorward of 40°S/N.

### 3.2.4 Vertical Transport

One contribution to the interhemispheric transport biases in the model could, among other factors, be related to differences in convective transport in the northern tropics and subtropics. In particular, Orbe et al. (2019) showed that the  $\Gamma_{\text{NHMID}}$  differences among the CCMI models were well correlated with the strength of northern subtropical convection. While their focus was on the strength of (parameterized) convection over the subtropical *oceans*, it is nonetheless still useful to also examine the simulated distributions of the radon tracer, despite the fact that it can only be credibly validated over land, owing to the limited available observations.

Given its short life-time (half-life of 3.8 days), Rn-222 is most responsive to rapid transport, such as that associated with convection. However, in evaluating the factors shaping the Rn-222 distribution one has to consider the consequences of convection on the circulation as well the direct impact of convective transport itself. By rapidly redistributing heat and momentum, convection induces meridional and zonal circulations which can then also advect radon. At low elevations, turbulence/dry convection act to redistribute radon away from its surface source.

Five-year average model profiles of Rn-222 are shown in Figure 7e for a location coincident with a set of two observations (12°N, 76°E). In the low and mid troposphere E2.1 exhibits larger values than the two E2.2 models which produce equivalent results. Analysis shows that this is due to greater gain by turbulence/dry convection and meridional transport in E2.1, which more than balance the greater loss by convective transport. At the same time, this greater convective transport promotes increased values above 4km compared with the other models. It is also worth noting that the (high) bias in E2.1 at this latitude occurs in exactly the same altitude range where E2.1 exhibits excessive water vapor (R20, Figure 33) and stronger moist convective mass fluxes, compared to E2.2(-AP) (R20, Figure 35). The two different observed profiles (Rani et al., 2014), one from early in the morning and one early in the afternoon are also shown in Fig. 7e (all

713 results are normalized to be equal to 1 at the surface). Given the disparity in data sam-  
 714 ple sizes, however, no meaningful comparison is possible, although taken at face value  
 715 the E2.2 models produce profiles whose time-average is similar to that shown in the ob-  
 716 served profile. Clearly, more tropical and subtropical Rn-222 observations are needed to  
 717 more credibly evaluate model convection and circulation in these regions.

718 A comparison of these models with Rn-222 observations was also made over north-  
 719 ern midlatitudes (Murray et al. (2014), shown in Supplementary Figure 7); the obser-  
 720 vations are averages of three or more data retrievals for each month. The results do not  
 721 indicate a consistent model high bias at either low or high elevations, with model val-  
 722 ues exceeding observations in the upper troposphere in some months, while the reverse  
 723 is true in others. The Rn-222 distribution above 8 km at these latitudes results from gain  
 724 by convection and resolved vertical advection, and loss by meridional transport. From  
 725 month-to-month the balance between these processes changes; thus, for example, the mod-  
 726 els have large values in the upper troposphere in July associated with large gains from  
 727 convection and resolved vertical advection, and in September due to less loss from merid-  
 728 ional transport. In August smaller values occur, from greater meridional transport loss  
 729 and smaller convective and resolved vertical transport gains. Ultimately these variations  
 730 result from the monthly/model differences in convection, but the complexity of this di-  
 731 agnosis is partly due to having convection in its own subroutine outside of the model’s  
 732 numerical solution of the conservation equations, resulting in air mass and tracer trans-  
 733 port fragmented between the two different subroutines.

734 Finally, Orbe et al. (2019) showed that convection over the subtropical oceans is  
 735 associated with both less efficient transport to high northern latitudes and faster inter-  
 736 hemispheric transport to high southern latitudes. The fact that the transports to high  
 737 latitudes are very similar between E2.1 and E2.2(-AP) therefore indicates that the (small)  
 738 differences in convection over land do not influence interhemispheric transport in E2.1/E2.2.

## 739 4 Dynamical and Transport Responses to Idealized Increases in CO<sub>2</sub>

740 Having validated the large-scale transport characteristics of E2.2(-AP) in the pre-  
 741 vious sections next we document changes in the stratospheric and tropospheric trans-  
 742 port circulations in response to both abrupt and transient increases in CO<sub>2</sub> through use  
 743 of the CMIP6 DECK experiments (Table 1). Following Grise and Polvani (2016) we term  
 744 the changes in the dynamical circulation the “dynamical sensitivity” of the model and,  
 745 by extension, those in the transport circulation the “transport sensitivity.”

746 The dynamical responses in the E2.2(-AP) CO<sub>2</sub> experiments were discussed only  
 747 briefly in R20, specifically with regards to changes in global mean surface temperature  
 748 and the response of the North Atlantic meridional overturning circulation. The only study  
 749 examining the stratospheric response so far (Ayarzagüena et al., 2020) only did so with  
 750 respect to stratospheric polar vortex variability (i.e. sudden warming events). Therefore,  
 751 though not exhaustive in our analysis, here we take the opportunity to present basic mea-  
 752 sures of the stratospheric and tropospheric dynamical responses that were not examined  
 753 in the previous studies but are important for interpreting the transport response, which  
 754 is the focus of this study. All responses ( $\delta$ ), which herein are defined as the difference  
 755 between the last 50 years of the abrupt and transient CO<sub>2</sub> simulations, relative to the  
 756 PI control, are discussed in the text and summarized accordingly in Table 3.

### 757 4.1 Stratospheric Dynamical and Transport Circulations

#### 758 4.1.1 Residual Mean Circulation ( $\Psi^*$ )

759 The residual mean circulation ( $\Psi^*$ ), here used to describe the advective component  
 760 of the Brewer-Dobson circulation, accelerates throughout the stratosphere as CO<sub>2</sub> is in-



creased (Fig. 8, top), a change that is among the more robust dynamical responses in models (Rind et al., 1998, 2002; Butchart & Scaife, 2001; Sigmond et al., 2004; Garcia & Randel, 2008; Li et al., 2008; Oberländer et al., 2013; Butchart et al., 2010; Hardiman et al., 2014). While in more realistic climate change scenarios changes in ozone depleting substances may significantly weaken this projected acceleration over the 21<sup>st</sup> century (Polvani et al., 2018; Abalos et al., 2019) it is nonetheless important that the underlying CO<sub>2</sub>-induced response of the BDC be rigorously understood.

The changes in the residual mean circulation manifest in the lower stratosphere as an increase in annual mean upwelling ( $\omega^*$ ) throughout the tropics and subtropics ( $\sim 20^\circ\text{S}$ - $20^\circ\text{N}$ ) (Fig. 8, bottom). In particular, lower stratospheric upwelling increases by  $17\pm 7.4\%$ ,  $16\pm 8.8\%$  and  $39\pm 9.7\%$  for 1%CO<sub>2</sub>, 2xCO<sub>2</sub>, and 4xCO<sub>2</sub>, respectively (Table 3, row 2). At higher altitudes (10 hPa) the changes  $\delta\omega^*$  are much smaller, at  $5.4\pm 13\%$  (1%CO<sub>2</sub>),  $4.2\pm 12\%$  (2xCO<sub>2</sub>), and  $8.4\pm 13\%$  (4xCO<sub>2</sub>). Overall, the good correspondence between the changes in  $\Psi^*$  ( $\omega^*$ ) between the 1%CO<sub>2</sub> and 2xCO<sub>2</sub> experiments indicates that the (equilibrated) acceleration of the circulation is not sensitive to the functional form of the prescribed CO<sub>2</sub> forcing (Fig. 8 left two panels, top and bottom). Note that 2xCO<sub>2</sub> levels are reached around year 70 of the 1%CO<sub>2</sub> integration. Furthermore, the fact that the 4xCO<sub>2</sub> response is nearly double that of the response in the 2xCO<sub>2</sub> experiment throughout the stratosphere indicates that the circulation scales approximately linearly with CO<sub>2</sub>, at least within the radiative forcing spanned by the range of CO<sub>2</sub> perturbations considered in this study.

Comparison of the fully coupled 2xCO<sub>2</sub> and 4xCO<sub>2</sub> experiments with those in the FIXSST experiments indicates the extent to which the residual circulation changes reflect rapid adjustments versus changes induced by SST warming. In the lower stratosphere (70 hPa), the response in upwelling is dominated by feedbacks associated with changes in SSTs, as indicated by the changes in  $\delta\omega^*$  for the fixed-SST simulations, which are equal to only 2.4% and 5.2% for 2xCO<sub>2</sub> and 4xCO<sub>2</sub>, respectively, compared to 16% and 39% for the fully coupled simulations (Table 3, row 2). By comparison, in the middle stratosphere (10 hPa) the values  $\delta\omega^*$  for the fixed-SST runs (3.9% (2xCO<sub>2</sub>) and 7.8% (4xCO<sub>2</sub>)) are much more comparable to the upwelling response in the fully coupled system (5.4% (2xCO<sub>2</sub>) and 8.4% (4xCO<sub>2</sub>)). Therefore, in the middle stratosphere rapid adjustments contribute significantly more to the circulation response compared to in the lower stratosphere, where SST changes play a key role in modulating the full coupled response.

#### 4.1.2 Stratospheric Transport Circulation ( $\delta\Gamma_{\text{STRAT}}$ and $\delta e90$ )

The response of the transport circulation is consistent with increases in the residual mean circulation (Fig. 9). Specifically, the mean age of air (Fig. 9, top) decreases throughout the stratosphere; at the same time, e90 (Fig. 9, bottom) increases throughout the tropical lower and middle stratosphere and over the midlatitude lower stratosphere, with large positive anomalies straddling the tropopause. The responses in both tracers are qualitatively consistent with Butchart and Scaife (2001), Butchart et al. (2010), and Oman et al. (2009), for the case of the mean age, and Abalos et al. (2017) (see their Figure 8), for the case of e90, albeit for the more comprehensive forcings considered in those studies.

Over the tropics the transport changes are consistent in amplitude with the increases in upwelling ( $\omega^*$ ), with values of  $\Gamma_{\text{STRAT}}$  in the tropical lower stratosphere decreasing by  $21\pm 8.3\%$ ,  $22\pm 8.2\%$ , and  $40\pm 7.5\%$  for 1%CO<sub>2</sub>, 2xCO<sub>2</sub>, and 4xCO<sub>2</sub>, respectively (Table 3, row 3). At the same time e90 increases by  $26\pm 9.7\%$  (1%CO<sub>2</sub>),  $26\pm 11\%$  (2xCO<sub>2</sub>) and  $54\pm 12\%$  (4xCO<sub>2</sub>) (Table 3, row 4). In addition to being consistent in magnitude with the changes in upwelling (Table 3, row 2), the transport responses in the tropics are also

811 generally linear with CO<sub>2</sub> (Table 3, column 4 vs. 5) and insensitive to the transient na-  
 812 ture of the forcing (Table 3, column 2 vs. 3).

813 Over higher latitudes in the lower stratosphere, the behavior of the mean age and  
 814 e90 tracers are also linear across the 2x- and 4xCO<sub>2</sub> experiments (Table 3, rows 5-6), al-  
 815 though a bit weaker in amplitude compared to the tropics, with  $\Gamma_{\text{STRAT}}$  decreasing by  
 816  $24 \pm 8.1\%$  poleward of 60°N (compared to 40% in the tropics) for the 4xCO<sub>2</sub> simulation  
 817 (Table 3, rows 5) and e90 poleward of 60°N increasing by  $32 \pm 8.9\%$ , compared to  $54 \pm 12\%$   
 818 in the tropics (also for 4xCO<sub>2</sub>). This weaker response at high latitudes reflects the fact  
 819 that the extra-tropical transport properties are not solely controlled by changes in trop-  
 820 ical advection, but also by mixing between the tropics and extra-tropics, with enhanced  
 821 mixing resulting in older mean ages over high latitudes (Neu & Plumb, 1999). In addi-  
 822 tion, as shown in Abalos et al. (2019) the high latitude changes in lower stratospheric  
 823 e90 are to a large extent tethered to changes in tropopause height, which rises in response  
 824 to increased CO<sub>2</sub>, as discussed further in the next section. Therefore, both changes in  
 825 extra-tropical mixing and tropopause height likely modulate the amplitude of the high  
 826 latitude e90 response to increased CO<sub>2</sub>.

827 Interestingly, while the mean state of the stratospheric transport circulation scales  
 828 more or less linearly with CO<sub>2</sub>, the transport variability changes nonlinearly, especially  
 829 in the tropics (Fig. 10). In particular, the amplitude of interannual variability in  $\Gamma_{\text{STRAT}}$   
 830 in the 4xCO<sub>2</sub> simulation (shown after the tracer response has more-or-less equilibrated)  
 831 underestimates that predicted by linearity by more than 50% in the tropics (Fig. 10b)  
 832 and 25% over high latitudes (Fig. 10a,c). This is consistent with a weakening in the am-  
 833 plitude of the Quasi-Biennial Oscillation as CO<sub>2</sub> increases (Supplementary Figure 8). Note  
 834 that, unlike changes in the period of the QBO, the weakening in QBO amplitude is a ro-  
 835 bust response among models as CO<sub>2</sub> increases, as documented in Richter et al. (2019)  
 836 for models participating in the SPARC Quasi-Biennial Oscillation initiative (QBOi), al-  
 837 though the implications for transport were not explored in that study. While our pre-  
 838 sentation here has been brief in keeping with the broad scope of this study, future work  
 839 will focus on further disentangling the role of the QBO in E2.2 on simulated transport  
 840 variability in the stratosphere and its response to climate change.

841 Finally, we exploit the abruptness of the CO<sub>2</sub> forcings in the 2xCO<sub>2</sub> experiment  
 842 to glean insight into the relationship between the changes in upwelling over the tropics  
 843 and the responses of  $\Gamma_{\text{STRAT}}$  (and e90) (Fig. 11). In particular, the evolution of global  
 844 mean  $\Gamma_{\text{STRAT}}$  (e90) at 70 hPa is shown to negatively (positively) covary closely with lower  
 845 stratospheric tropical upwelling (correlations  $> 0.8$ , Fig. 11 a,b). Furthermore, the evo-  
 846 lution of the upwelling and transport responses are observed to hold not only on inter-  
 847 annual timescales but also in the initial SST-mediated response to CO<sub>2</sub> that occurs within  
 848 the first 10-15 years after the forcing is applied. Given the important role of SST changes  
 849 in the upwelling response, illustrated earlier through use of the fixed-SST experiments,  
 850 we also find that the tropical upwelling responsible for the transport changes are strongly  
 851 correlated with the changes in tropical SST warming (Fig. 11c).

## 852 4.2 Tropospheric Dynamical and Transport Circulations

### 853 4.2.1 Tropospheric Dynamical Circulation ( $\delta\Psi^*$ , $\delta p_{\text{trop}}$ and $\delta\text{MCFLX}$ )

854 First we consider the changes in the residual mean streamfunction in the tropo-  
 855 sphere (Fig. 12, top). (Note we do not use more conventional (Eulerian) measures for  
 856 the mean meridional circulation (MMC) because, as in the stratosphere, our discussion  
 857 is oriented around changes in the transport circulation, for which the residual mean cir-  
 858 culation is most relevant). Overall, the changes in  $\Psi^*$  reflect a narrowing and acceler-  
 859 ation in the mid-to-upper tropical troposphere in agreement with Li et al. (2010), ac-  
 860 companied by a deceleration and weakening throughout the midlatitude troposphere in  
 861 both hemispheres. As with the stratospheric transport and dynamical changes, the changes

862 in the abrupt 2xCO<sub>2</sub> integration are very similar and almost identical to those produced  
863 in the transient forcing run.

864 Unlike in the stratosphere, comparisons of (double) the 2xCO<sub>2</sub> changes in  $\delta\Psi^*$  with  
865 those from 4xCO<sub>2</sub> reveal much weaker linearity in both hemispheres. This is generally  
866 consistent with Marvel et al. (2015) who show that precipitation responds nonlinearly  
867 in ModelE to different anthropogenic forcings, albeit for a broad range of trace gas and  
868 aerosol forcings used in that study (as opposed to the incremental CO<sub>2</sub> increases con-  
869 sidered here). In particular, we find that in the NH (SH)  $\delta\Psi^*$  decreases in the 4xCO<sub>2</sub>  
870 simulation by  $4.9\pm 4.6\%$  ( $9.2\pm 4.6\%$ ), compared to the 14% (5.1%) predicted by linear-  
871 ity (Table 3 row 7). Interestingly, the nonlinearity in  $\delta\Psi^*$  is more pronounced over the  
872 extra-tropics, compared to the tropics, where one may expect that abrupt changes in con-  
873 vective instability may drive nonlinear behavior in the overturning tropical circulation.  
874 Rather, over the extra-tropics the nonlinear behavior in  $\delta\Psi^*$  may be related to non-monotonic  
875 changes in baroclinic eddies with increasing surface air temperature, as has been explored  
876 in O’Gorman and Schneider (2008), albeit using an idealized model.

877 In particular, further inspection of the baroclinic eddy kinetic energy generation  
878 reveals significant nonlinear (and non-monotonic) behavior, especially over the NH, with  
879 hemispherically averaged values at 500 hPa decreasing from  $53.1\times 10^{-4}$  W/m<sup>2</sup>/hPa in  
880 the PI control to  $52.0\times 10^{-4}$  W/m<sup>2</sup>/hPa in the 2×CO<sub>2</sub> experiment and then increasing  
881 to  $54.5\times 10^{-4}$  W/m<sup>2</sup>/hPa for 4×CO<sub>2</sub>. Though beyond the scope of this study, future work  
882 will focus on exploring nonlinearities in the midlatitude eddy-driven circulation more rig-  
883 orously through use of a broader suite of CO<sub>2</sub> forcing experiments spanning 0.5-to-8×CO<sub>2</sub>.

884 As the mean meridional circulation weakens and expands the tropopause rises in  
885 response to increased CO<sub>2</sub> (Fig. 12, black lines) (Lorenz & DeWeaver, 2007; Lu et al.,  
886 2008). Over the tropics the tropopause rises by  $6.3\pm 1.8\%$ , and  $6.3\pm 2.0\%$  and  $13\pm 2.1\%$   
887 for the 1%CO<sub>2</sub>, 2xCO<sub>2</sub> and 4xCO<sub>2</sub> experiments, respectively; the extra-tropical response  
888 ( $\delta p_{\text{trop}}$ ) is similar in magnitude, if not slightly weaker (Table 3, rows 7-8). The tropopause  
889 height changes over both the tropics and extra-tropics scale approximately linearly with  
890 CO<sub>2</sub> as do the (parameterized) convective mass flux changes  $\delta\text{MCFLX}$  (Fig. 12, bottom),  
891 which decrease throughout most of the troposphere (excluding the upper troposphere  
892 and the Arctic), as predicted by theoretical constraints on the mass exchange between  
893 the boundary layer and free troposphere (Held & Soden, 2006). (Note that the latter changes  
894 are primarily linked not to a reduction in the zonal-mean overturning (i.e. the Hadley  
895 circulation) but, rather, a reduction in the zonally asymmetric Walker circulation (Vecchi  
896 & Soden, 2007)). In the next section we discuss what the different responses between  
897 the MMC, tropopause height and mass flux measures imply for the tropospheric trans-  
898 port circulation responses to increased CO<sub>2</sub>.

#### 899 **4.2.2 Tropospheric Transport Circulation ( $\delta\chi_{\text{NH},5/50}$ and $\delta\Gamma_{\text{NHMID}}$ )**

900 In response to a doubling of CO<sub>2</sub> the changes in the loss tracers  $\chi_{\text{NH},5}$  (Fig. 13 top)  
901 and  $\chi_{\text{NH},50}$  (Fig. 13 middle) consist primarily of weakly negative anomalies (5-10%) through-  
902 out the troposphere and a band of positive anomalies at the tropopause. The pattern  
903 and magnitude of the response of  $\chi_{\text{NH},50}$  strongly resembles that of the response of an  
904 idealized air-mass origin tracer presented in Orbe et al. (2015) (see their Figure 3) and  
905 the idealized tracer  $\chi_{\text{CO},50}$  analyzed among the ACCMIP models in Doherty et al. (2017),  
906 albeit for the different scenarios (Ref A1b and RCP 6.0, respectively) considered in those  
907 studies. Furthermore, while the increased burdens of the surface loss tracers at the tropopause  
908 could be interpreted merely as reflections of increased tropopause height, Doherty et al.  
909 (2017) (see their Figure 11) showed that the tracer increases persist even after replot-  
910 ting in “tropopause-relative” coordinates. This suggests that the CO<sub>2</sub> induced changes,  
911  $\delta\chi_{\text{NH},5}$  and  $\delta\chi_{\text{NH},50}$ , are not simply reflections of tropopause height changes but, rather,

912 also reflect changes in along-isentropic transport in the troposphere to high latitudes,  
 913 as discussed in Orbe et al. (2015).

914 Comparisons of  $\delta\chi_{\text{NH},5/50}$  for the 2xCO<sub>2</sub> and 4xCO<sub>2</sub> experiments indicates that  
 915 the transport response in the troposphere is nonlinear with increased CO<sub>2</sub>. In partic-  
 916 ular, for  $\chi_{\text{NH},5}$  the response to 4xCO<sub>2</sub> is significantly weaker ( $-7.1\pm 2.2\%$ ) than twice the  
 917 response to a doubling of CO<sub>2</sub> ( $-11\%$ ) (Table 3, row 11). This behavior is much more  
 918 consistent with the nonlinear behavior in the MMC ( $\delta\Psi^*$ ), compared to the linear changes  
 919 in extra-tropical convective mass fluxes and tropopause height discussed earlier. There-  
 920 fore, while vertical mass flux changes have been invoked in previous studies to qualita-  
 921 tively interpret the transport response to climate change (Fang et al., 2011; Doherty et  
 922 al., 2017) our results suggest that the driving mechanism more likely involves a weak-  
 923 ening of the (resolved) mean meridional circulation.

924 Finally, the response of  $\Gamma_{\text{NHMID}}$  to a doubling of CO<sub>2</sub> consists of small ( $\sim 5\%$ ) pri-  
 925 marily positive anomalies throughout the Southern Hemisphere (Fig. 13, bottom). (Note  
 926 that the decreases in  $\Gamma_{\text{NHMID}}$  above the tropopause mirror those for  $\Gamma_{\text{STRAT}}$ , discussed  
 927 in the previous section). The fact that  $\Gamma_{\text{NHMID}}$  increases is consistent with an overall weak-  
 928 ening of the MMC and with Holzer and Boer (2001), who showed that interhemispheric  
 929 exchange times, mixing times, and mean transit times all increase by 10% in response  
 930 to a doubling of CO<sub>2</sub>. The fact that the response in E2.2-AP is weaker is likely not re-  
 931 lated to our use of  $\Gamma_{\text{NHMID}}$  as a measure of IHT, given that Holzer and Boer (2001) also  
 932 used similar integrated measures derived from the age spectrum (Hall & Plumb, 1994;  
 933 Holzer & Hall, 2000). Rather, the differences most likely reflect differences in the under-  
 934 lying models, particularly with respect to resolution as well as their sea surface temper-  
 935 ature response to increasing CO<sub>2</sub>; both of these affect the simulated transport sensitiv-  
 936 ity (Rind et al., 2002). Though beyond the scope of this current study, future work will  
 937 focus on further understanding how the transport sensitivity in E2.2 varies with reso-  
 938 lution, choice of convective parameterization, coupling to the ocean and other factors.

## 939 5 Sensitivity Analysis

940 Here we comment on the sensitivity experiments introduced in Section 2 that guided  
 941 the development of the “Altered Physics (AP)” version of E2.2 (i.e. E2.2-AP). In par-  
 942 ticular, various aspects of the convective parameterization were altered in order to re-  
 943 move artificial dependence on layer thickness, including changes made to detrainment,  
 944 conditional instability, repartitioning of precipitation into lofted and detrained fractions,  
 945 evaporating precipitation, downdrafts and updrafts. Upon incorporation of some of the-  
 946 ses changes Rind et al. (2020) showed that E2.2-AP differs from E2.2 in several respects  
 947 (e.g. convective mass flux, specific humidity, precipitation, standing wave number 1 en-  
 948 ergy in the stratosphere). Those differences notwithstanding, however, here we have shown  
 949 that the large-scale transport properties of the two model versions are nonetheless very  
 950 similar, at least relative to the larger existing differences between E2.2 and E2.1. Next  
 951 we show that this is because, unlike in previous “Middle Atmosphere” versions of Mod-  
 952 elE, E2.2-AP was developed explicitly with transport considerations in mind.

953 More precisely, E2.2-AP was developed so as to produce not only a credible QBO  
 954 period as in past versions (Rind et al., 2014) but also a realistic stratospheric mean age  
 955 of air. As discussed in R20 the QBO period is relatively straightforward to tune by al-  
 956 tering the assigned convective phase velocities and convection/momentum flux scaling  
 957 within the non-orographic gravity wave drag parameterization. By comparison, the strato-  
 958 spheric mean age, as illustrated in the previous sections (see Figure 11), is strongly teth-  
 959 ered to the (resolved) upwelling in the tropical lower stratosphere, which in turn is highly  
 960 dependent on the model’s climatological SSTs. Therefore, upon introducing some of the  
 961 convective parameterization changes in the (atmosphere-ocean) coupled version of E2.2

962 we found that the associated increases in SSTs resulted in increased lower stratospheric  
 963 upwelling, which in turn directly affected the stratospheric mean age in the model.

964 In particular, Fig. 14a shows how applying the proposed convection changes in both  
 965 coupled (atmosphere-ocean) and AMIP versions of E2.2 results in a vertical redistribu-  
 966 tion of climatological mean convection to more “top-heavy” profiles (R20). While this  
 967 is consistent with the original intention of the proposed changes (i.e. to produce a warmer  
 968 upper tropical troposphere, considering that E2.2 is biased cold in the troposphere), the  
 969 SSTs in the coupled (atmosphere-ocean) system also adjust accordingly, increasing by  
 970  $\sim 2$  degrees, with some changes producing larger SST responses (red, blue, cyan) com-  
 971 pared to others (green). (Note that, by design, these changes to the convective param-  
 972 eterization produce similar mass flux responses in the AMIP configurations, but with no  
 973 associated changes in SSTs).

974 As the SSTs increase in response to the convective parameterization changes, lower  
 975 stratospheric upwelling also increases in the coupled simulations (Fig. 14b), a feedback  
 976 that is absent in the AMIP experiments. These increases in lower stratospheric upwelling  
 977 are driven by an equatorward shift in the subtropical upper tropospheric jet, which in-  
 978 creases the equatorward Eliassen-Palm flux convergence occurring in the lower stratosphere  
 979 in both hemispheres from  $45^\circ\text{S}$  to  $45^\circ\text{N}$  (not shown). A similar jet-mediated pathway  
 980 linking warmer SSTs to increased upwelling has been reported in previous studies includ-  
 981 ing Rind et al. (2002) and Li et al. (2010), among others.

982 Associated with these changes in the large-scale flow the QBO periods in the cou-  
 983 pled simulations also increase (large filled circles, Fig. 14c). While retuning the non-orographic  
 984 GWD can correct for the QBO period changes (small filled circles) the large-scale flow  
 985 changes nonetheless persist and are associated with significantly younger stratospheric  
 986 mean ages, compared to in the AMIP experiments (Fig. 14d). Therefore, in determin-  
 987 ing which convection changes were to be incorporated in E2.2-AP we decided only on  
 988 those that produced *both* QBO periods and mean age values consistent with observations  
 989 (green filled circles, Fig. 14).

990 The above illustrates two important aspects of the development of E2.2(-AP). The  
 991 first relates to optimizing the model not only in terms of its middle atmospheric dynam-  
 992 ics but also its transport circulation (mean age). The second relates to the critical role  
 993 played by testing various parameterization settings in both AMIP and coupled atmosphere-  
 994 ocean configurations. In particular, the latter captures feedbacks between convection,  
 995 sea surface temperatures and stratospheric upwelling that cannot be gleaned in a pre-  
 996 scribed SST framework but are nonetheless key for evaluating the true coupled nature  
 997 of the model.

## 998 6 Conclusions

999 The main goal of this study has been to evaluate the large-scale transport char-  
 1000 acteristics of the new climate model GISS-E2.2 that has been specially optimized for the  
 1001 middle atmosphere and whose output has been contributed to the CMIP6 archive. As  
 1002 such it complements the overview presented in Rind et al. (2020), which discussed in de-  
 1003 tail the model’s underlying structure, parameterization choices (including departures from  
 1004 those chosen in the lower vertical resolution version of ModelE (E2.1)), and a broad range  
 1005 of key dynamical and radiative properties of the model’s climatology. As in that study,  
 1006 in addition to validating the performance of the model over the historical period, we also  
 1007 present its climate response, with the goal of quantifying the “transport sensitivity” of  
 1008 E2.2 through use of the abrupt  $4\times\text{CO}_2$  experiment submitted to CMIP6 as well as ad-  
 1009 ditional  $\text{CO}_2$  varying (i.e.  $2\times\text{CO}_2$  and  $1\%\times\text{CO}_2$ ) experiments. Finally, we present results  
 1010 from several sensitivity tests in order to illustrate the large-scale dynamical and trans-

1011 port assessments that were used to inform the parameterized convective and non-orographic  
 1012 gravity wave drag settings that were employed in E2.2-AP.

1013 Our analysis of a broad range of transport measures derived from both real chemical  
 1014 as well as idealized tracers shows various improvements in the stratospheric transport  
 1015 circulation in E2.2 compared to previous versions of the model. Most notably, the  
 1016 stratospheric mean age values in E2.2 represent a dramatic improvement over previous  
 1017 model versions in which the mean ages were too young (Shindell et al., 2013) and likely  
 1018 reflect the weaker tropical ascent in the model as well as a more realistic tropical pipe.  
 1019 In addition to these improvements in the mean state of the stratospheric transport cir-  
 1020 culation, the transport variability associated with the QBO is also captured in the dis-  
 1021 tributions of various tracers (i.e. CH<sub>4</sub>, O<sub>3</sub>) owing to the incorporation of non-orographic  
 1022 GWD drag sources from convection and shear that are absent in other versions of Mod-  
 1023 elE.

1024 For sake of completeness we have also presented a (brief) evaluation of the tro-  
 1025 pospheric transport climate in E2.2, which shows similar overall characteristics to those  
 1026 of E2.1. While both versions of the model exhibit somewhat too vigorous poleward trans-  
 1027 port in the Northern Hemisphere, which may be related to a systematic upward bias in  
 1028 the midlatitude jet, the overall properties of the tropospheric transport climate are within  
 1029 the range spanned by other chemistry climate models, particularly those recently partic-  
 1030 ipating in CCMI.

1031 Our validation of E2.2 against both observations and the CCMI models indicate  
 1032 that it is a model well equipped for use in understanding not only recent past but also  
 1033 future changes in the transport circulation. To this end, we have also presented an eval-  
 1034 uation of the “transport sensitivity” of E2.2 that goes beyond the standard DECK set  
 1035 of CMIP6 integrations by including a 2xCO<sub>2</sub> experiment as well as fixed SST versions  
 1036 of the abrupt 2xCO<sub>2</sub> and 4xCO<sub>2</sub> experiments. From the former we have assessed the lin-  
 1037 earity of the transport circulation response to CO<sub>2</sub> and from the latter we have quan-  
 1038 tified the relative importance of rapid adjustments versus feedbacks to both dynamical  
 1039 and transport responses. Our main findings are as follows:

- 1040 • In response to doubled (quadrupled) CO<sub>2</sub>, E2.2 simulates a ~20% (~40%) reduc-  
 1041 tion in the stratospheric mean age and increases in e90 in the tropical lower strato-  
 1042 sphere, consistent in magnitude and sign with enhanced upwelling in the tropi-  
 1043 cal lower stratosphere.
- 1044 • Over the entire stratosphere the transport responses in both  $\Gamma_{\text{STRAT}}$  and e90 scale  
 1045 approximately linearly with CO<sub>2</sub> and with SST warming in the tropics.
- 1046 • Increases in lower stratospheric upwelling are driven primarily by SST warming,  
 1047 with rapid adjustments playing a minor role (< 30%). By comparison, rapid ad-  
 1048 justments play a much more important role at higher altitudes (10 hPa).
- 1049 • In the troposphere E2.2 simulates increased burdens of NH midlatitude surface  
 1050 tracers over the Arctic high latitude tropopause, accompanied by decreased bur-  
 1051 dens over midlatitudes as CO<sub>2</sub> increases. This response is nonlinear with CO<sub>2</sub>, con-  
 1052 sistent with nonlinear changes in the residual mean meridional circulation. By com-  
 1053 parison, changes in tropopause height and vertical mass exchange by (parameter-  
 1054 ized) convection are much more linear.

1055 While the exact magnitude of the transport responses in E2.2 are likely to depend  
 1056 on the specifics of the model (e.g. resolution, convective parameterization) the overall  
 1057 responses in both the stratospheric and tropospheric tracers are consistent in magnitude  
 1058 and pattern with the results from previous studies. In particular, the changes in  $\Gamma_{\text{STRAT}}$   
 1059 and e90 respectively point to an acceleration of the Brewer-Dobson circulation and en-  
 1060 hanced stratosphere-troposphere exchange over both the tropics and extra-tropics. In  
 1061 the troposphere the changes in the idealized loss and mean age tracers are indicative of

1062 enhanced Arctic burdens of NH midlatitude surface tracers and (weak) reductions in interhemispheric transport.  
1063

1064 A novel contribution from this study is that we have explicitly evaluated the linearity of the transport circulation response in both the stratosphere and the troposphere to increased CO<sub>2</sub>. This is motivated partly by the results from a recent study by Abalos et al. (2019) who showed strong correlations between the projected changes in stratosphere-troposphere transport and the amplitude of upper tropospheric warming in the CCM1 models (see their Figure 2), indicating the potential for using upper troposphere/lower stratosphere transport measures to constrain climate sensitivity. Here, through use of different CO<sub>2</sub> forcing experiments, we have shown that this relationship also exists in E2.2, in which the stratospheric transport circulation response is strongly correlated with the amplitude of surface warming.  
1073

1074 Given the broad scope of this study we have only evaluated the transport circulation and sensitivity of E2.2 in the absence of composition feedbacks through use of the non-interactive version of the model. Given that stratospheric ozone feedbacks can play an important role in modulating “dynamical sensitivity” (Chiodo & Polvani, 2017), however, it remains to be seen how the “transport sensitivity” of E2.2 itself depends on how ozone and other constituents evolve as the planet warms. To this end, interactive versions of E2.2 have also been produced for CMIP6 and will be presented in future studies.  
1081

## 1082 **7 Data Availability**

1083 All E2.1 and E2.2-AP CMIP6 DECK simulations discussed in this study are available through the Earth System Grid Federation (ESGF). In addition, all of the E2.2 sensitivity and fixed-SST experiments can be found at <https://gmao.gsfc.nasa.gov/gmaoftp/corbe/CMIP6/E2-2-G/>.  
1086

## 1087 **Acknowledgments**

1088 C.O. thanks Krzysztof Wargan for processing and performing quality screening on the MLS Aura N<sub>2</sub>O fields that were used in this analysis, Darryn Waugh for providing the in-situ SF<sub>6</sub> age profiles and HALOE tape-recorder phase lag values, and Eric Fleming for help with accessing the ground-based total column ozone measurements. Climate modeling at GISS is supported by the NASA Modeling, Analysis and Prediction program, and resources supporting this work were provided by the NASA High-End Computing (HEC) Program through the NASA Center for Climate Simulation (NCCS) at Goddard Space Flight Center.  
1095

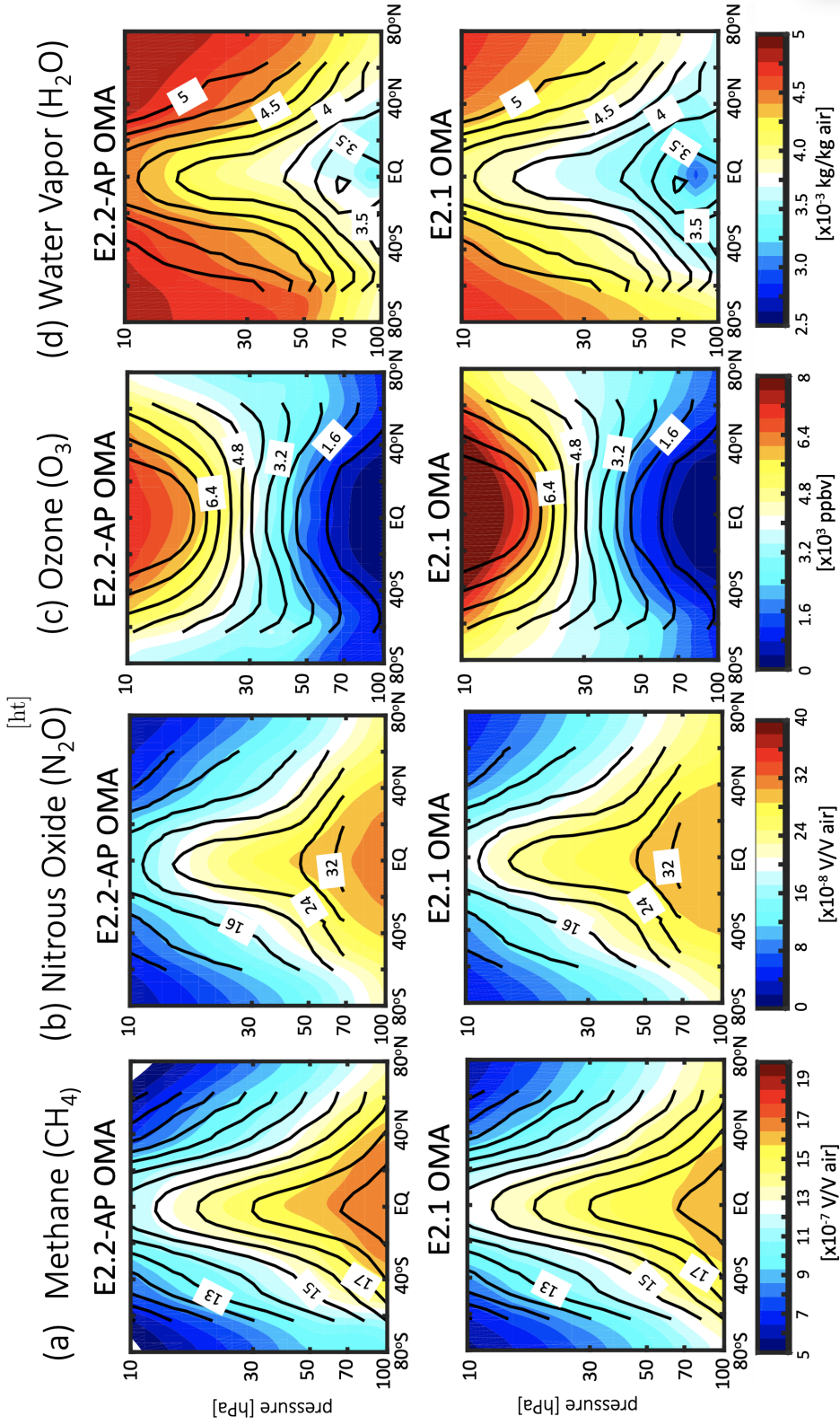


**Figure 1.** Climatological annually and zonally averaged methane (a) ( $\text{CH}_4$ ), (b) nitrous oxide ( $\text{N}_2\text{O}$ ), (c) ozone ( $\text{O}_3$ ) and (d) water vapor ( $\text{H}_2\text{O}$ ). Color contours shows the three-member mean of the E2.2-AP OMA Historical ensemble (top) and the two-member mean of the E2.1 OMA Historical ensemble (bottom). Black contours show observed values from HALOE (a,c,d) and MLS (b). Climatologies have been performed over years 1991-2002 when comparing to HALOE (a,c,d) and over 2005-2014 when comparing to MLS (b).



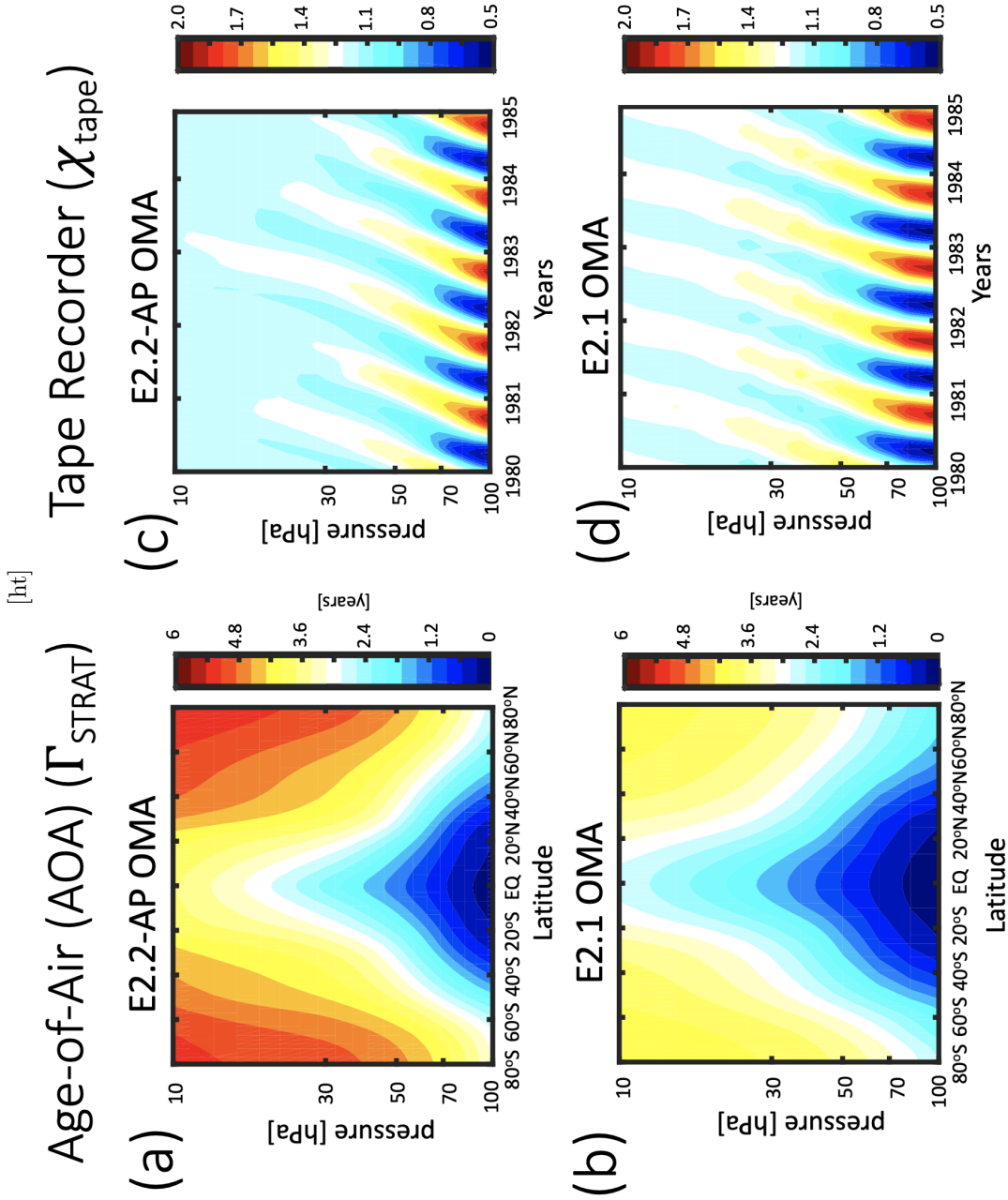


**Figure 2.** Left: Zonal and annually averaged climatological stratospheric mean age of air ( $\Gamma_{\text{STRAT}}$ ), averaged over the last five years (2010-2014) of the E2.2-AP (a) and E2.1 (b) OMA Historical ensembles, respectively. Three (two) members are included in the E2.2-AP (E2.1) ensemble means. Right: Evolution of the 10°S-10°N averaged zonal mean tape-recorder tracer ( $\chi_{\text{tape}}$ ) for E2.2-AP (c) and E2.1 (d). Note the faster ascent characteristics in E2.1, compared to E2.2-AP. Only one member of E2.1 is shown in (d) in order to avoid averaging over (offset) oscillations.

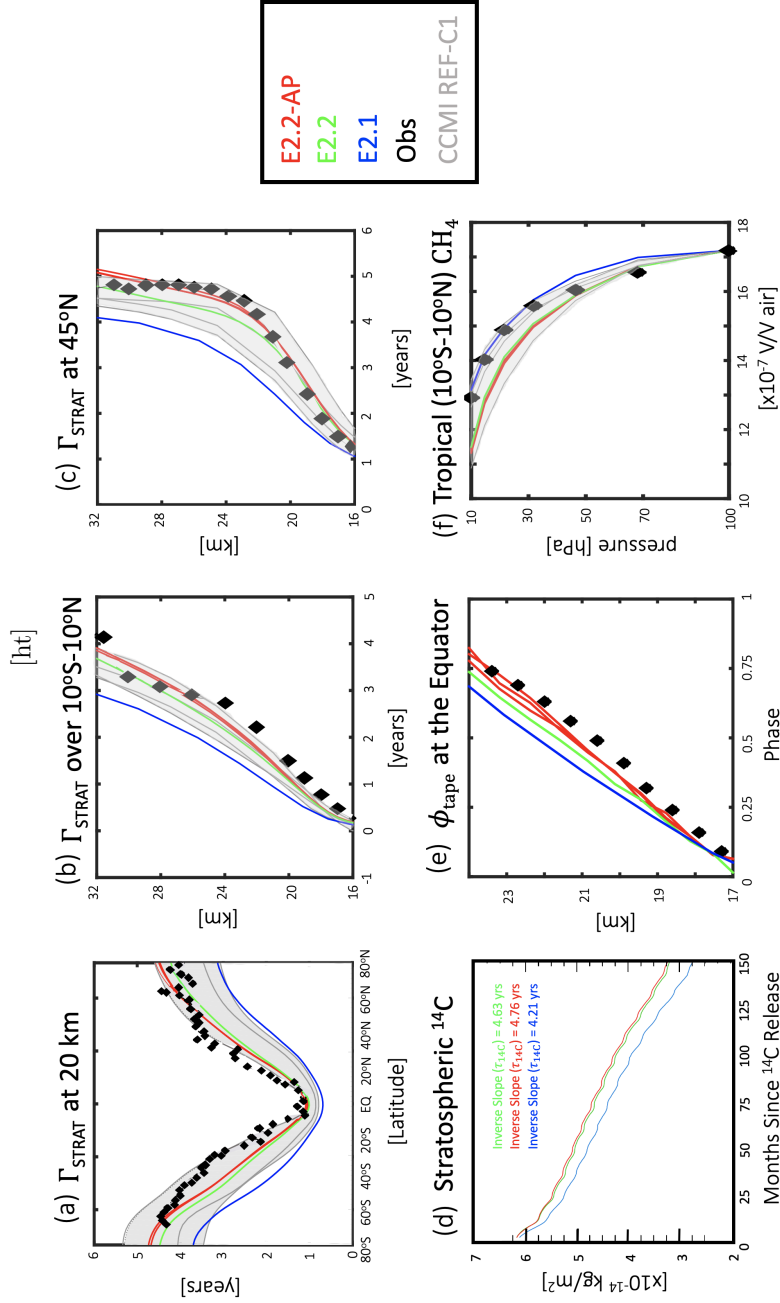


**Figure 3.** (a) Meridional profile of the stratospheric mean age of air ( $\Gamma_{\text{STRAT}}$ ) at 20 km. Vertical profiles of  $\Gamma_{\text{STRAT}}$ , averaged over 10°S-10°N (b) and evaluated at 45°N (c). The evolution of the (natural log of the) stratospheric mass of  $^{14}\text{C}$  is shown in (d), along with the associated stratospheric residence time, inferred as the (inverse) slope after 100 months. Vertical profiles over the tropics (10°S-10°N) of the “tape recorder” phase lag, as inferred from a tape recorder tracer ( $\chi_{\text{tape}}$ ) and methane ( $\text{CH}_4$ ) (f), normalized to values at the lowest HALOE level, are also shown. Color lines in all panels denote three ensemble members of E2.2-AP (red), one member of E2.2 (green), and two members of E2.1 (blue) while grey shading denotes the range spanned by the CCM1 models (grey lines denote individual models). In-situ based estimates are shown in the black diamonds for  $\Gamma_{\text{STRAT}}$  (a-c),  $\chi_{\text{tape}}$  (e) and  $\text{CH}_4$  (f).

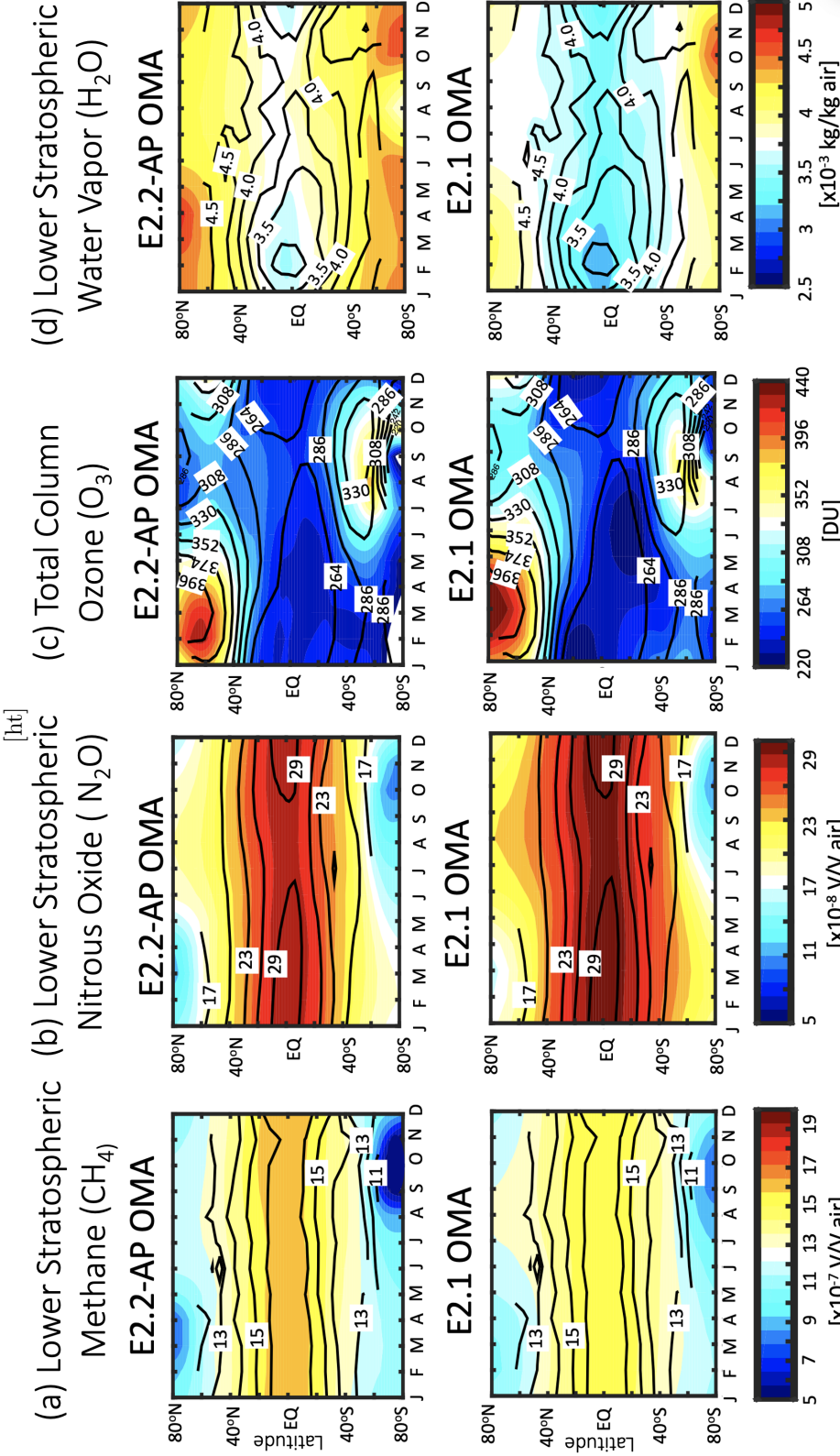


**Figure 4.** Seasonal cycle of zonally averaged methane (a) ( $\text{CH}_4$ ), (b) nitrous oxide ( $\text{N}_2\text{O}$ ), (c) ozone ( $\text{O}_3$ ) and (d) water vapor ( $\text{H}_2\text{O}$ ), further averaged over the middle-to-lower stratosphere (30-100 hPa). For the case of ozone (c) the total column is shown. Color contours shows the three-member mean of the E2.2-AP OMA Historical ensemble (top) and one member of the E2.1 OMA Historical simulation (bottom). Black contours denote observed values from HALOE (a,d), AURA-MLS (b) and TOMS/OMI (c). Climatologies have been performed over years 1991-2002 when comparing to HALOE (a,d), over 2005-2014 when comparing to MLS (b) and over 2000-2010 when comparing to TOMS/OMI (c).

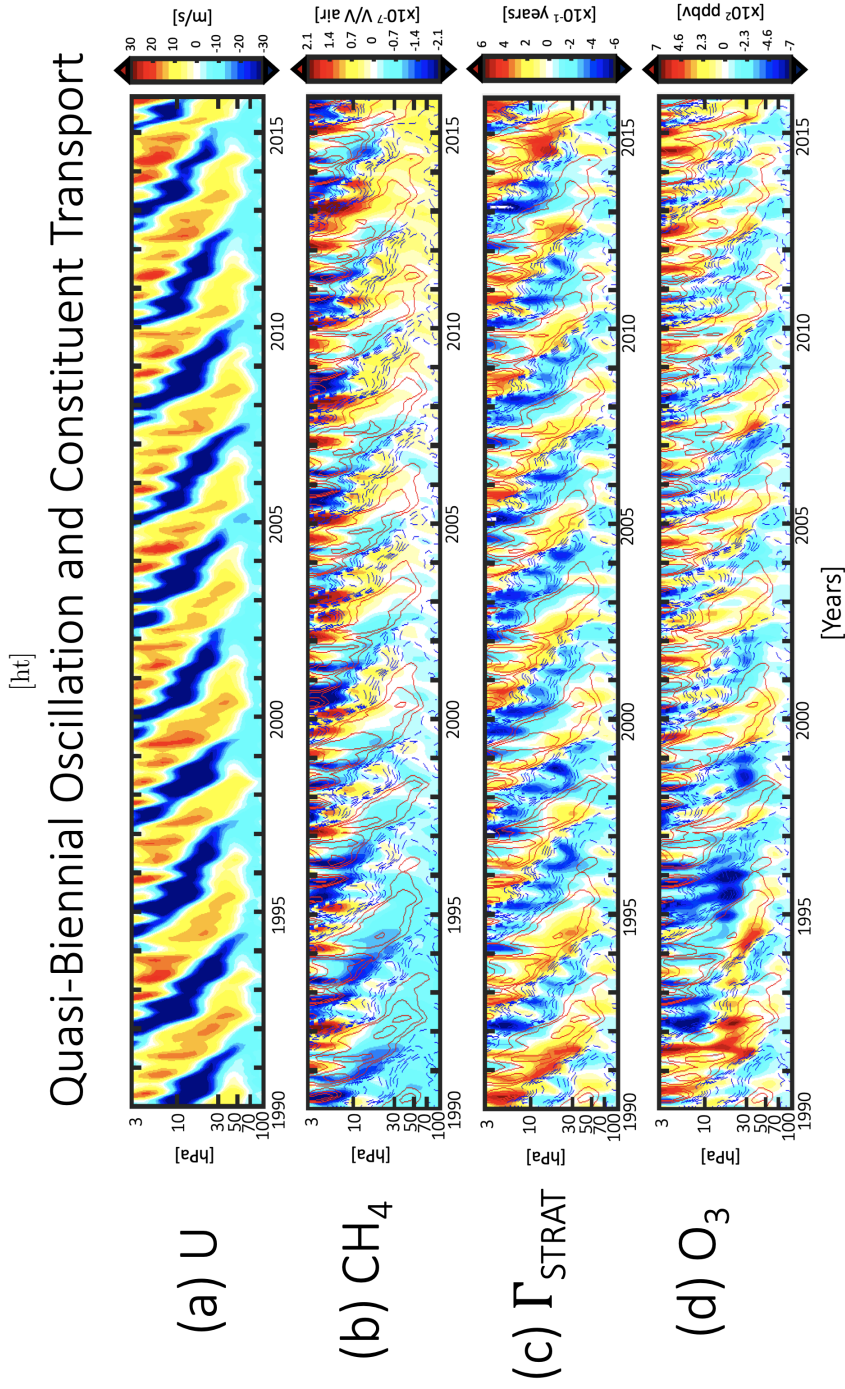


**Figure 5.** Dynamical and transport signatures of the Quasi-Biennial Oscillation in E2.2-AP as represented in terms of the near-equatorial ( $5^{\circ}S$ - $5^{\circ}N$ ) zonally averaged zonal winds (a) and in terms of climatological anomalies (relative to the 1990-2015 mean) of methane ( $CH_4$ ) (b), the stratospheric mean age of air ( $\Gamma_{STRAT}$ ) (c) and ozone ( $O_3$ ) (d). Only one ensemble member from the OMA E2.2-AP ensemble is shown so as not to average across different QBO phases among ensemble members. Red and blue contours in (b-d), spaced every 6 m/s, denote negative and positive zonal wind anomalies, respectively.

[ht]  
 Historical Annual Mean Total Column Ozone

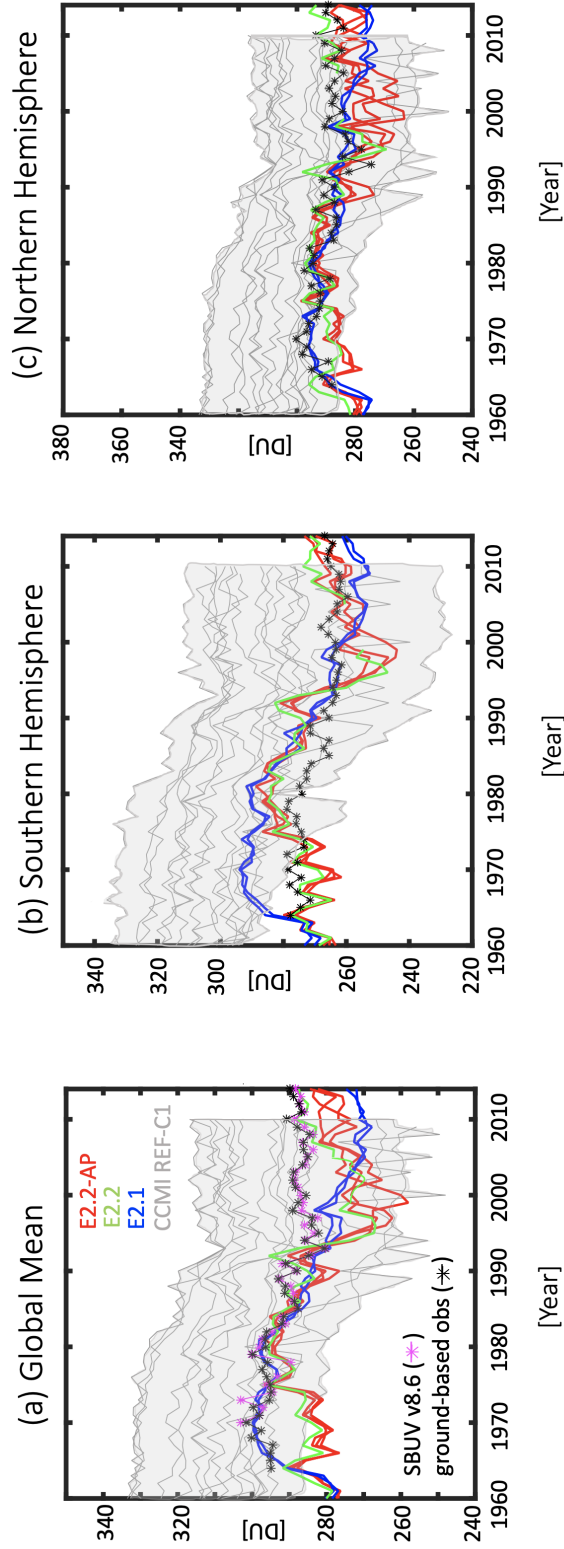


**Figure 6.** Total column ozone, globally averaged ( $90^{\circ}\text{S}$ - $90^{\circ}\text{N}$ ) (a) as well as averaged over the Southern Hemisphere (b) and over the Northern Hemisphere (c). Red, green and blue lines denote three ensemble members of E2.2-AP, one member of E2.2, and two members of E2.1, respectively. Grey shading denotes the range spanned by the CCMII models up through 2010, the final year of the REF-C1 experiment (grey lines denote individual models). Ground-based and the SBUV v8.6 merged satellite measurements of global mean total column ozone are shown in (a) in black and magenta, respectively.

[ht]  
2000-2010 Annual Mean Idealized Tropospheric Tracers

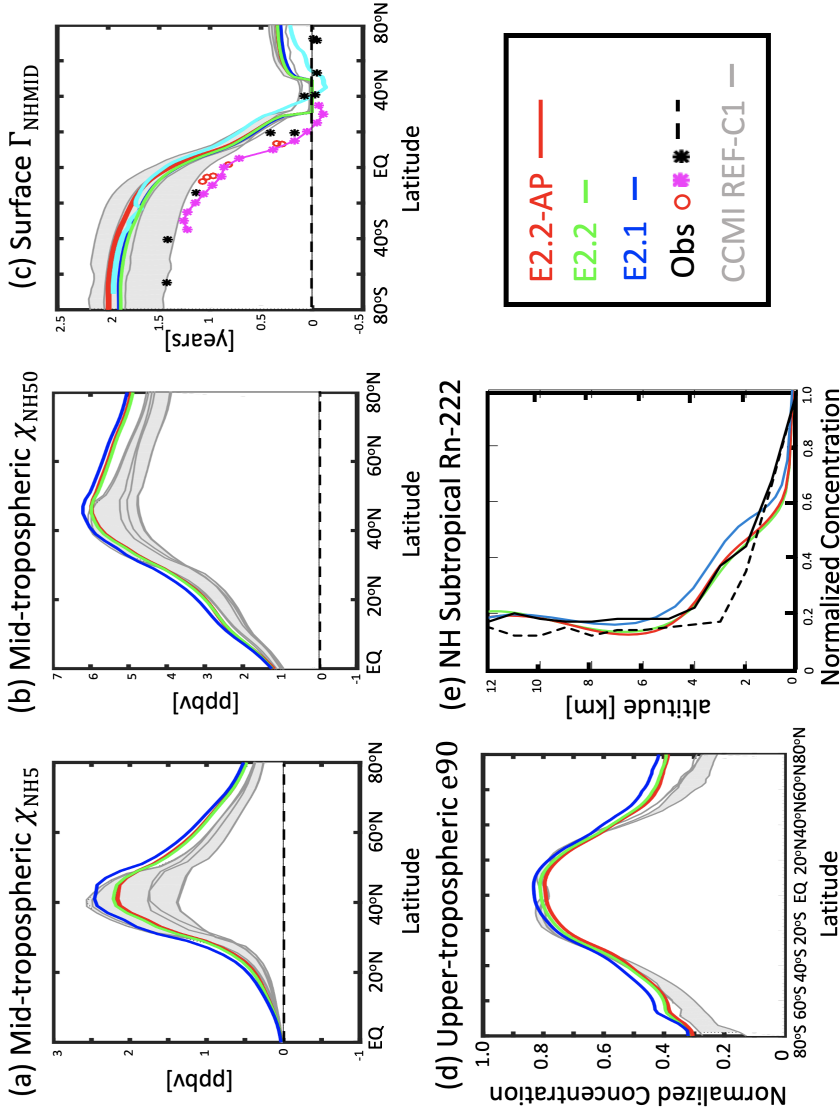


**Figure 7.** 2000-2010 annual mean climatological meridional profiles of the NH midlatitude surface loss tracers  $\chi_5$  and  $\chi_{50}$  at 500 hPa (a,b), the NH midlatitude mean age,  $\Gamma_{NHMD}$ , evaluated at 900 hPa (c), e90, averaged over 100-500 hPa, and normalized by its surface layer value (d), and northern subtropical profiles of the radon tracer (Rn-222), also normalized by values at the surface (e). Red, green and blue lines denote three ensemble members of E2.2-AP, one member of E2.2, and two members of E2.1, respectively, while grey shading shows the range spanned by the CCM1 models (grey lines denote individual models). (Note that Rn-222 was not available for the CCM1 models.) The cyan line in (c) denotes the  $SF_6$  age in E2.2-AP, which can be most directly compared to the observed ages (black, magenta, red symbols). For both the models and observations the  $SF_6$  age ( $a_{SF6}$ ) has been calculated as the time lag satisfying  $\chi(\mathbf{r}, t) = \chi_0(t - a_{SF6})$ .

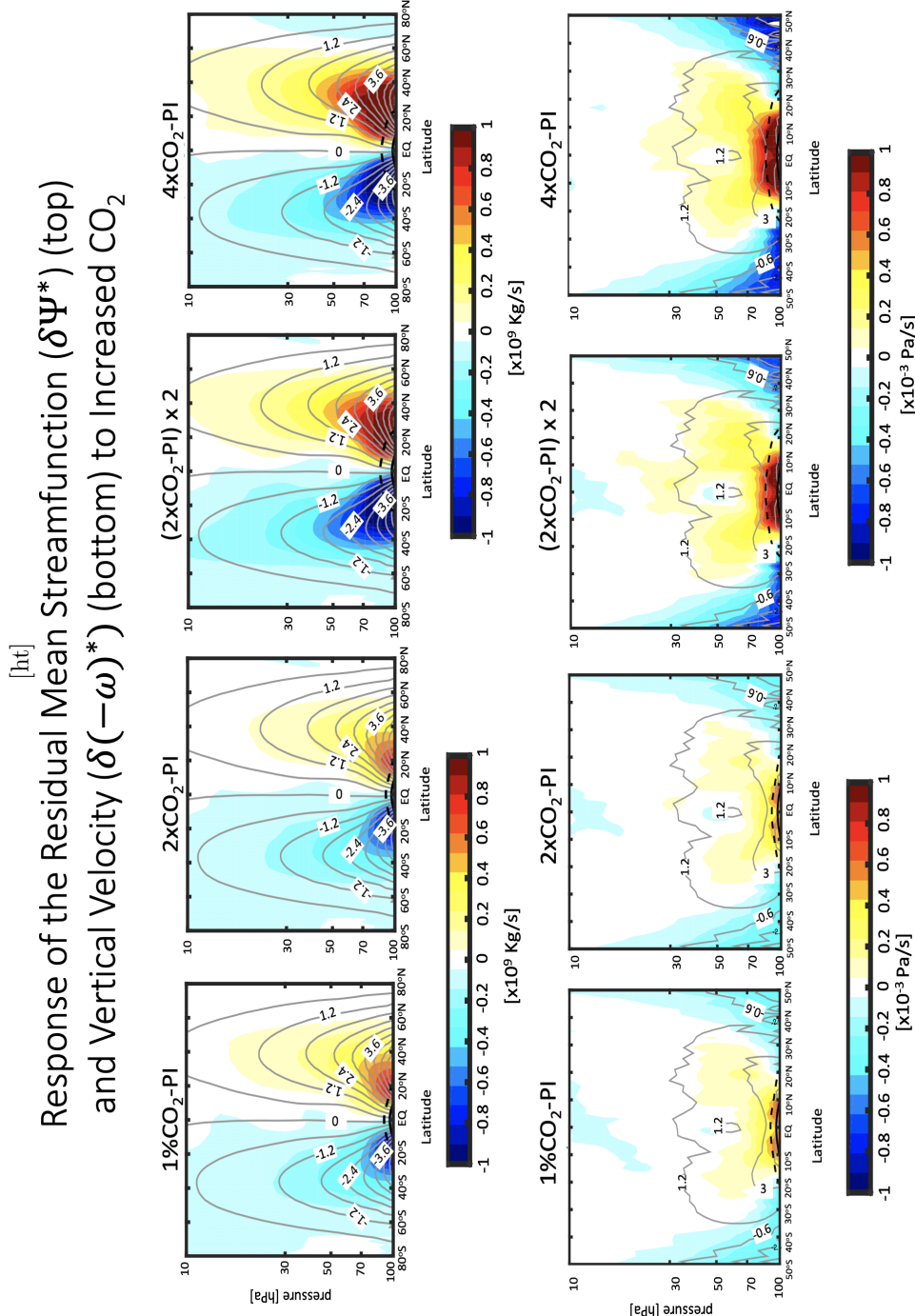


**Figure 8.** The simulated response in E2.2-AP of the residual mean streamfunction ( $\Psi^*$ ) (top) and vertical velocity ( $-\omega^*$ ) in the stratosphere (bottom) in response to increased CO<sub>2</sub>. Color contours show changes relative to the pre-industrial (PI) control for the 1%CO<sub>2</sub>, 2xCO<sub>2</sub> and 4xCO<sub>2</sub> simulations in the first, second and fourth columns, respectively. Grey contours show climatological values for the PI control. Comparisons of double the responses to 2xCO<sub>2</sub> (third column) with the panels in the fourth column indicate the degree to which the circulation responses are linear with CO<sub>2</sub> forcing. (Note that changes in upwelling are depicted in terms of  $-\omega^*$  in the bottom panels in order to reinforce the sense that the circulation is accelerating in response to increased CO<sub>2</sub>.)

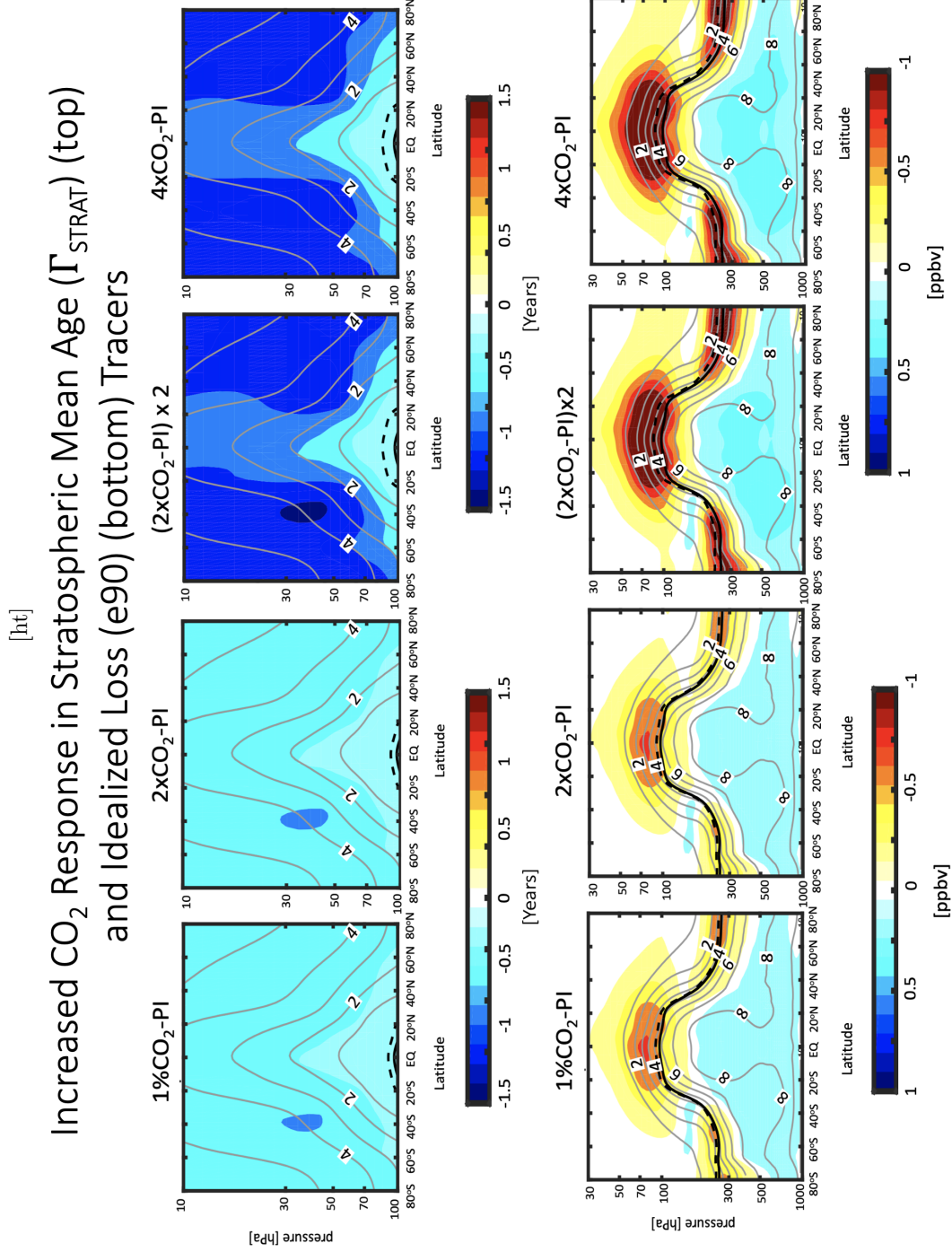


**Figure 9.** As in Figure 8, except now showing changes in the stratospheric mean age ( $\Gamma_{\text{STRAT}}$ ) (top) and e90 (bottom). The black dashed and solid thick lines show the climatological annually averaged tropopause for the increased CO<sub>2</sub> and PI control experiments, respectively. Grey contours show climatological values for the PI control.



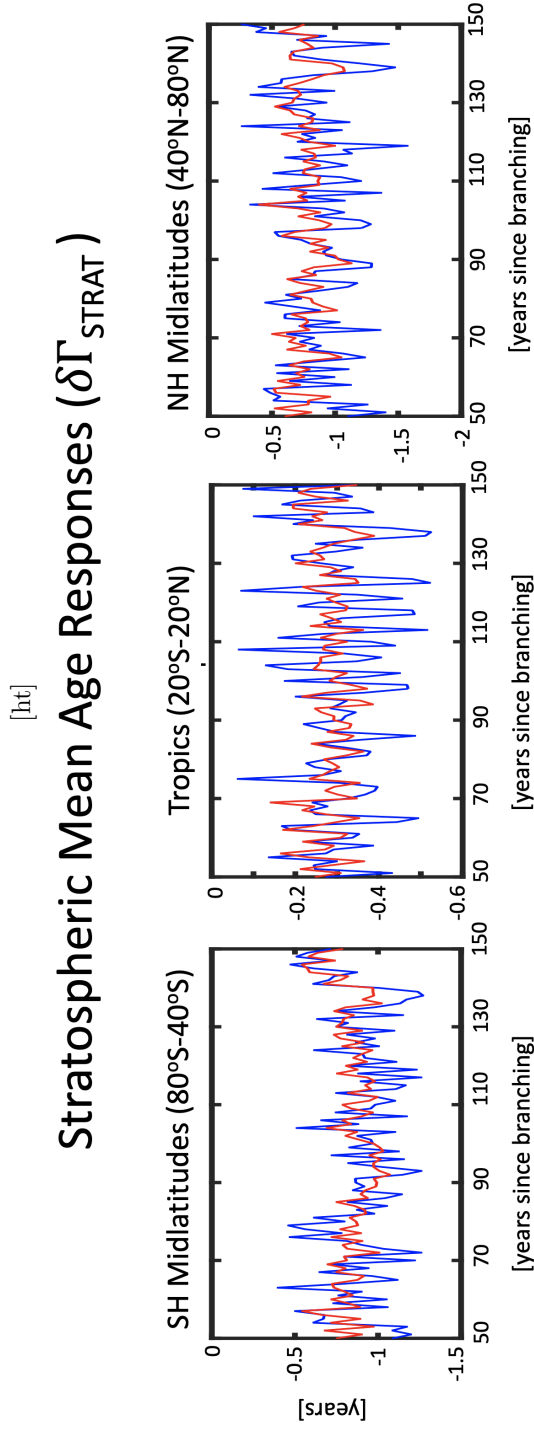


**Figure 10.** Evolution of changes in the stratospheric mean age of air,  $\Gamma_{\text{STRAT}}$ , relative to the PI control for (twice the) response to  $2\times\text{CO}_2$  (blue lines) and  $4\times\text{CO}_2$  (red lines). Results are shown for E2.2-AP for years 50-150 after branching from the underlying PI control. Latitudinal averages at 70 hPa have been performed over SH midlatitudes ( $80^\circ\text{S}-40^\circ\text{S}$ ) (left), the tropics ( $20^\circ\text{S}-20^\circ\text{N}$ ) (middle), and NH midlatitudes ( $40^\circ\text{N}-80^\circ\text{N}$ ) (right).

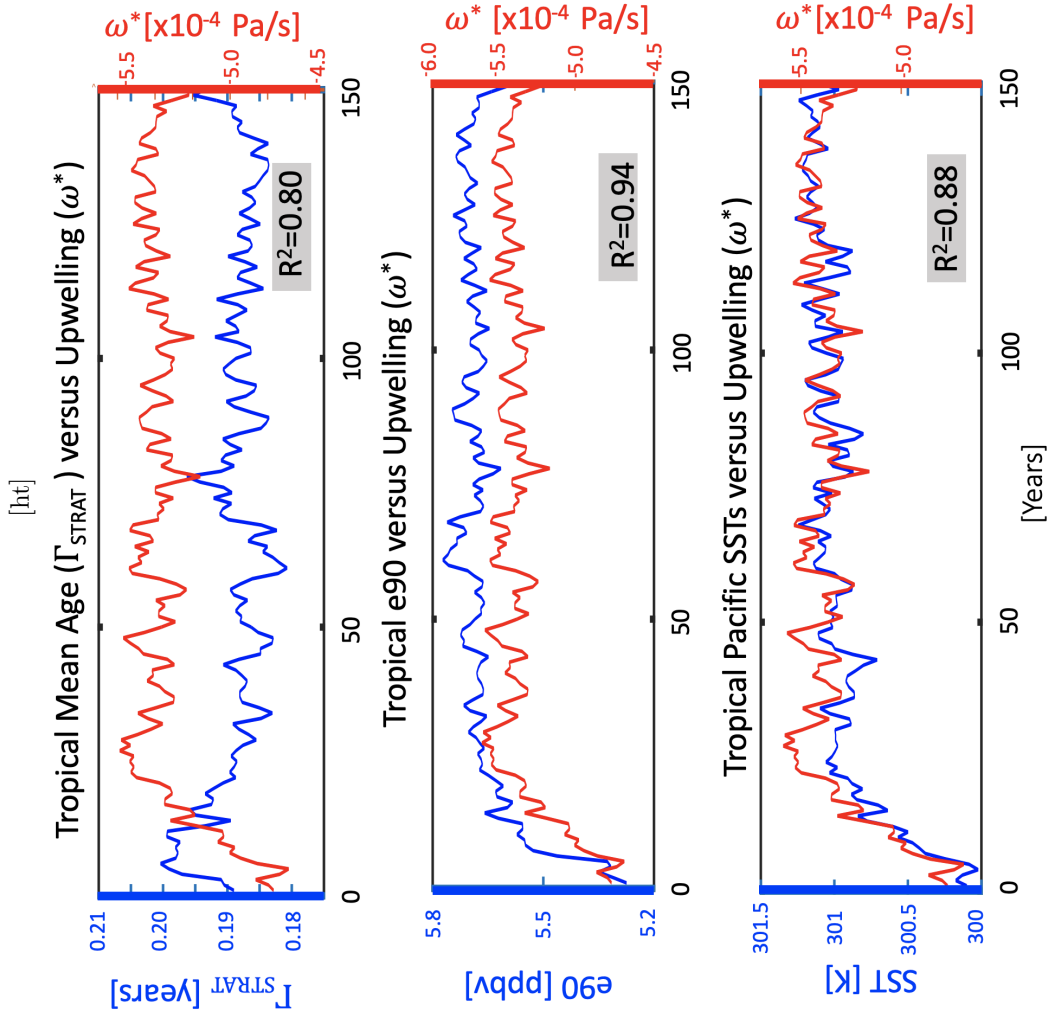


**Figure 11.** Evolution of lower stratospheric tropical upwelling in E2.2-AP (red lines) compared against the evolution of the stratospheric mean age ( $\Gamma_{\text{STRAT}}$ ) (blue line, top) and e90 (blue line, middle), also evaluated in the lower stratosphere (i.e. latitudes spanning  $10^\circ\text{S}$ - $10^\circ\text{N}$  at 70 hPa). The bottom panel compares the evolution of upwelling with tropical Pacific sea surface temperatures, averaged over  $10^\circ\text{S}$ - $10^\circ\text{N}$ . Correlations of the fields in each panel are shown in the bottom right-hand panels. Note that a four-year moving average has been applied to all timeseries.

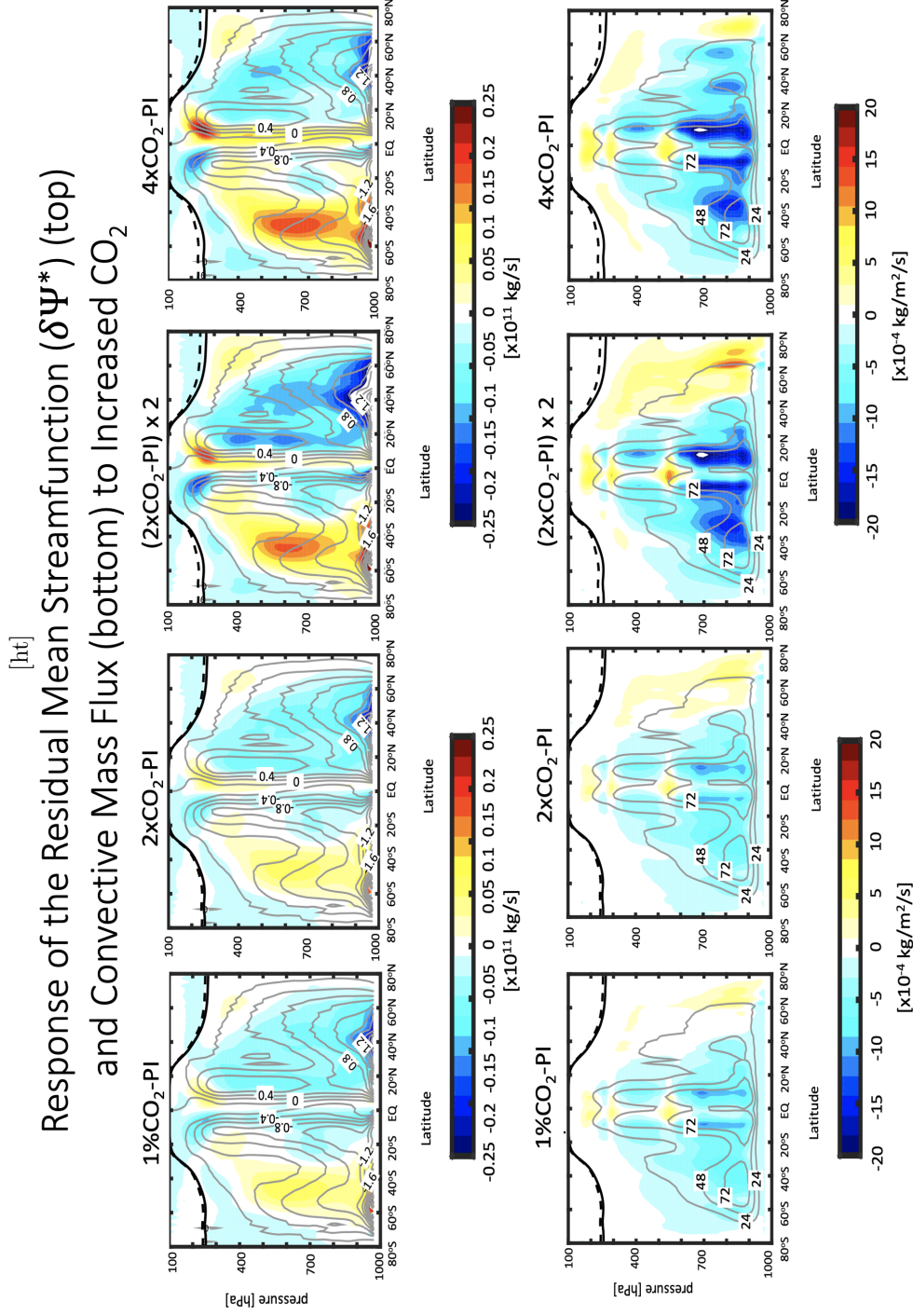


**Figure 12.** As in Figures 8 and 9, except showing annual mean changes in the residual mean circulation ( $\Psi^*$ ) evaluated in the troposphere (top) and vertical mass exchange due to (parameterized) convection (bottom), respectively. The black dashed and solid thick lines show the climatological annually averaged tropopause for the increased CO<sub>2</sub> and PI control experiments, respectively. As in previous figures results are shown for E2.2-AP and grey contours show climatological values for the PI control.

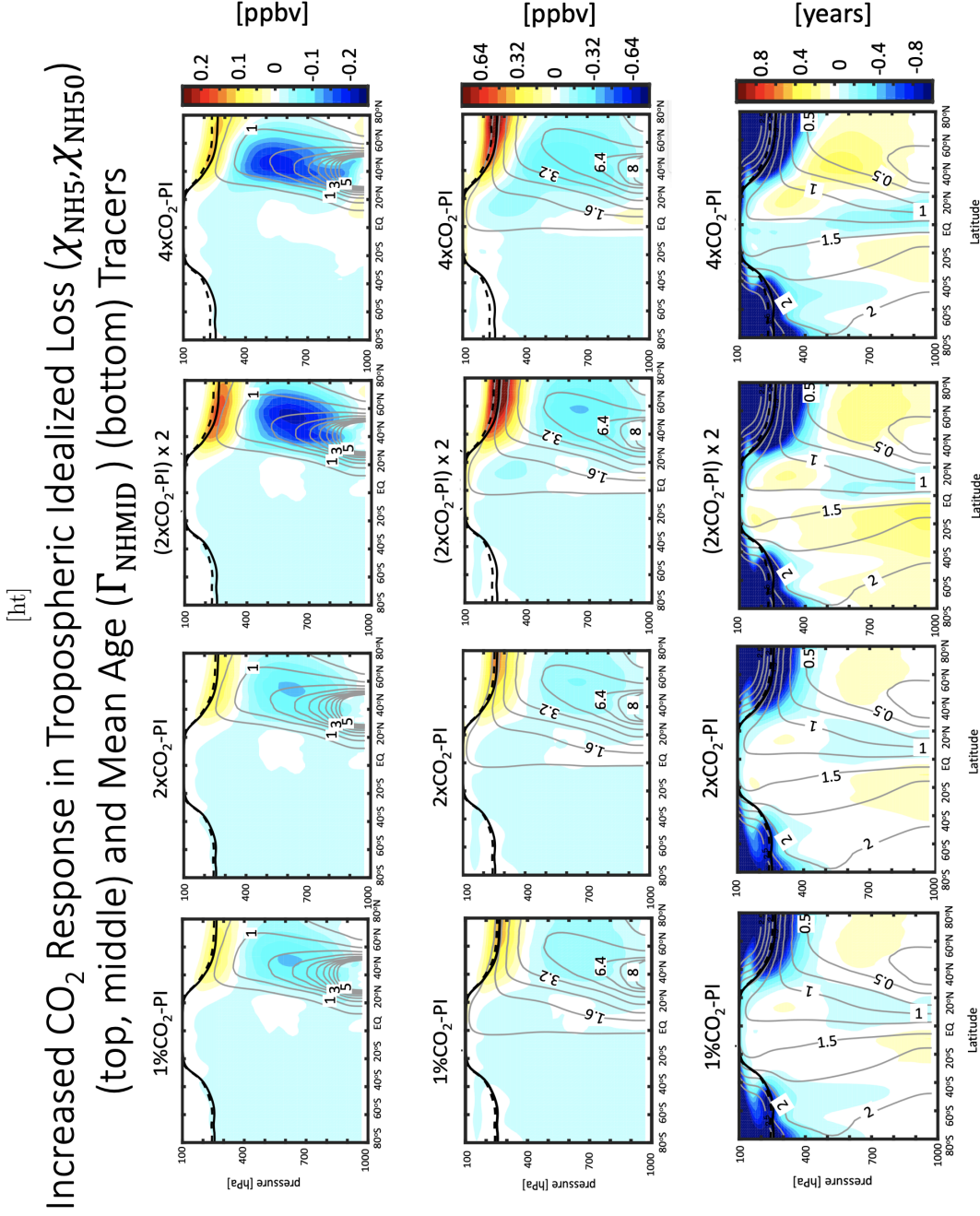


**Figure 13.** As in Figures 8, 9 and 12, except showing annual mean changes in the 5-day and 50-day idealized loss tracers,  $\chi_{\text{NH},5}$  (top) and  $\chi_{\text{NH},50}$  (middle), respectively. Changes in the mean transit time since air was last at the NH midlatitude surface ( $\Gamma_{\text{NHMID}}$ ) are shown in the bottom panels. The black dashed and solid thick lines show the climatological annually averaged tropopause for the increased CO<sub>2</sub> and PI control experiments, respectively. As in previous figures results are shown for E2.2-AP and grey contours show climatological values for the PI control.

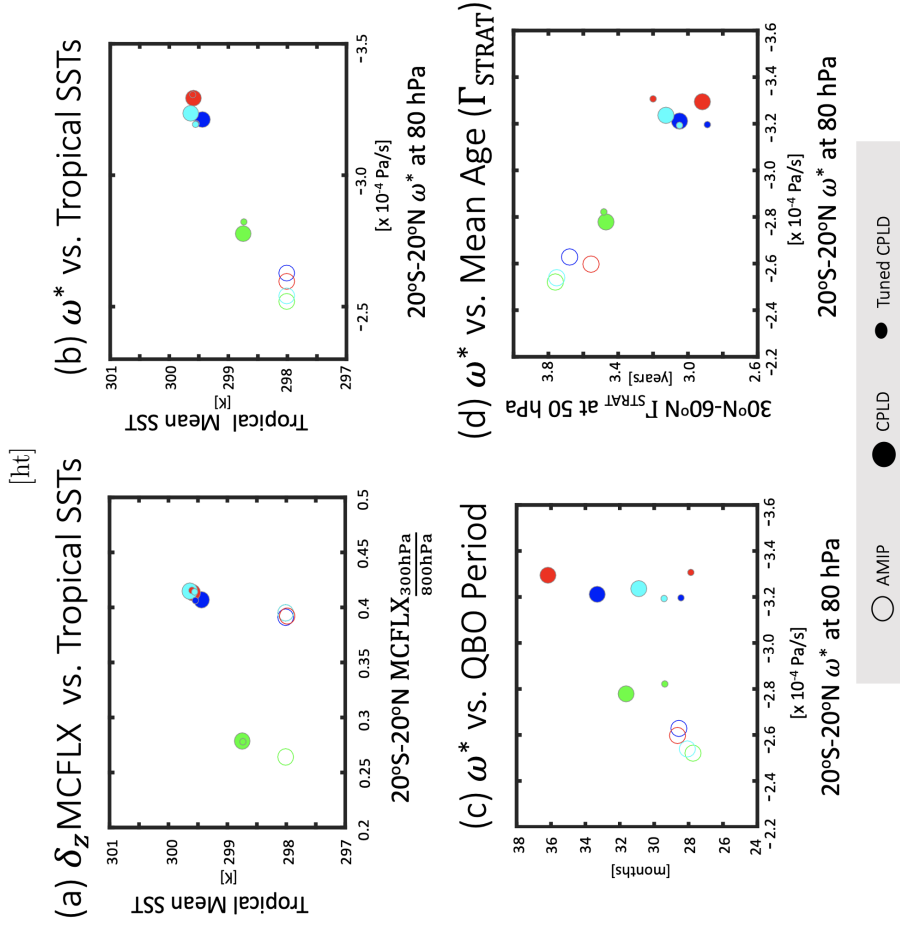


**Figure 14.** The relationship between climatological mean sea surface temperatures in the tropics and the 300/800 hPa ratio of the vertical mass exchange due to (parameterized) convection (a), tropical SSTs and lower stratospheric (LS) upwelling ( $\omega^*$  at 80 hPa averaged over  $20^\circ\text{S}-20^\circ\text{N}$ ) (b), LS upwelling and QBO period (c) and LS upwelling versus the NH midlatitude (stratospheric) mean age of air ( $\Gamma_{\text{STRAT}}$ ) at 50 hPa (d). Circles show various sensitivity experiments using E2.2 (Table 1, rows 10-11). Open (closed) circles denote AMIP (coupled atmosphere-ocean) simulations while green, red, blue and cyan correspond to individual experiment pairs. Large (small) filled circles denote the coupled runs prior to (after) tuning the QBO period.

**Table 1.** Experiments analyzed in this study described in terms of model version (Col.1), simulation type (Col.2), CMIP6 archive tag name (Col. 3; \*note some of the simulations were not submitted to CMIP6), simulation years (Col. 4) and number of ensemble members (Col. 5). Note that all of the historical AMIP and coupled PI control and CO<sub>2</sub> experiments are part of the GISS-E2.2-AP-G DECK submission to CMIP6. The historical AMIP simulation using E2.1 was also submitted to CMIP6. <sup>a</sup>-<sup>b</sup>Years 2000–2150 and 1850–2000 correspond to the 150 years following “branching” in the underlying PI control and CO<sub>2</sub> experiments, respectively. All trace gases and aerosols (except for CO<sub>2</sub>) are set to PI values. <sup>c</sup> Same as <sup>b</sup> except for only 30 years after branching. <sup>d</sup> Years 1850–1880 represent 30 years of perpetual PI (1850) conditions.

Model Version	Simulation Type	CMIP6 Archive Tag	Simulation Years	No. Ensemble Members
E2.2-AP	OMA Historical AMIP	GISS-E2-2-G.amip.r[1-3]i1p3fl	1850–2014	3
E2.2	OMA Historical AMIP	n/a*	1850–2014	1
E2.1	OMA Historical AMIP	GISS-E2-1-G.amip.r[1-2]i1p3fl	1850–2014	2
E2.2-AP	NINT Coupled Pre-Industrial	GISS-E2-2-G.piControl.r1i1p1fl	2000–2150 <sup>a</sup>	1
E2.2-AP	NINT Coupled 1%CO <sub>2</sub>	GISS-E2-2-G.1pctCO2.r1i1p1fl	1850–2000 <sup>b</sup>	1
E2.2-AP	NINT Coupled 2xCO <sub>2</sub>	GISS-E2-2-G.abrupt-2xCO2.r1i1p1fl	1850–2000 <sup>b</sup>	1
E2.2-AP	NINT Coupled 4xCO <sub>2</sub>	GISS-E2-2-G.abrupt-4xCO2.r1i1p1fl	1850–2000 <sup>b</sup>	1
E2.2-AP	NINT FIXSST 2xCO <sub>2</sub>	n/a*	1850–1880 <sup>c</sup>	1
E2.2-AP	NINT FIXSST 4xCO <sub>2</sub>	n/a*	1850–1880 <sup>c</sup>	1
E2.2 SENS AMIP 1-4	NINT Pre-Industrial AMIP	n/a*	1850–1880 <sup>d</sup>	4
E2.2 SENS Coupled 1-4	NINT Pre-Industrial Coupled	n/a*	1850–1880 <sup>d</sup>	4

**Table 2.** Observational products used for evaluating chemical and transport characteristics of E2.2-AP, E2.2 and E2.1 in terms of relevant tracer measure (Col. 1), process evaluated (Col. 2), product name (Col. 3) and reference(s) (Col. 4)

Tracer Metric	Process Evaluated	Observational Product	Reference
Zonal Mean CH <sub>4</sub> , N <sub>2</sub> O, O <sub>3</sub> , H <sub>2</sub> O	General Comparison	HALOE, MLS	(Groß & Russell, 2005)
Total Column O <sub>3</sub>	Seasonal Cycle and Historical Trends (1960-2014)	TOMS/OMI, WOUDC, SBUV v8.6	(R. McPeters et al., 2008; Fioletov et al., 2002) (R. D. McPeters et al., 2013)
Vertical Profile of Stratospheric CH <sub>4</sub>	Tropical-Midlatitude Mixing	HALOE	(Groß & Russell, 2005)
Stratospheric Tape Recorder ( $\chi_{\text{tape}}$ )	Tropical-Midlatitude Mixing and Ascent	HALOE	(Hall et al., 1999)
Stratospheric Mean Age ( $\Gamma_{\text{STRAT}}$ )	Stratospheric mean transport timescale	in-situ SF <sub>6</sub> and CO <sub>2</sub>	(Boering et al., 1996; Bönisch et al., 2009)
<sup>14</sup> C Residence Time	Stratospheric transport timescale	in-situ <sup>14</sup> C	(Prather & Remsberg, 1993)
Tropospheric Mean Age ( $\Gamma_{\text{NHMID}}$ )	Tropospheric interhemispheric transport timescale	SF <sub>6</sub> (HATS, CCGG)	(Waugh et al., 2013)
NH 5(50)-day Loss Tracers ( $\chi_{\text{NH},5/50}$ )	Midlatitude-Arctic transport	n/a	(Orbe et al., 2016, 2019)
Surface 90-day Loss Tracer (e90)	Upper Troposphere/Lower Stratosphere transport	n/a	(Abalos et al., 2017, 2019)
Radon Tracer (Rn-222)	Vertical Mixing	in-situ profiles	(Rani et al., 2014; Murray et al., 2014)

**Table 3.** The response (%) of different dynamical and transport measures in E2.2-AP (Col. 1) for 1%CO<sub>2</sub> (Col. 2), 2xCO<sub>2</sub> (Col. 3), and 4xCO<sub>2</sub> simulations (Col.5), relative to pre-industrial conditions. Col. 4 shows double the 2xCO<sub>2</sub> changes (Col. 3) in order to assess the linearity of different metrics' responses to increased CO<sub>2</sub>. Columns 6 and 7 show the responses from the Fixed-SST abrupt 2xCO<sub>2</sub> and 4xCO<sub>2</sub> experiments. (Note that the tracers were not integrated in those runs so that only dynamical fields are shown). TP, GB, ETP, POL and ARC denotes "tropical" (20°S-20°N), global (90°S-90°N), extra-tropical (30°S/N-60°S/N), polar (60°S/N) and Arctic (50°N-90°N), respectively. The vertical mass exchange due to (parameterized) convection is denoted by MCFLX. In row 7  $\Psi^*|_{\text{trop}}$  denotes the residual mean streamfunction evaluated in the troposphere at 500 hPa. Uncertainty is denoted as  $\pm\sigma$ , where  $\sigma$  is the standard deviation of the corresponding metric, evaluated over all 150 years.

Measure	$\delta 1\% \text{CO}_2$ [%]	$\delta 2x \text{CO}_2$ [%]	2x( $\delta 2x \text{CO}_2$ ) [%]	$\delta 4x \text{CO}_2$ [%]	$\delta 2x \text{CO}_2^{\text{FIXSST}}$ [%]	$\delta 4x \text{CO}_2^{\text{FIXSST}}$ [%]
TP (GB) SSTs	5.2(8.6)	5.3(9.2)	10(18)	11(15)	n/a	n/a
TP $\omega^*$ at 70(10) hPa	17 $\pm$ 7.4 (5.4 $\pm$ 13)	16 $\pm$ 8.8(4.2 $\pm$ 12)	33(8.3)	39 $\pm$ 9.7 (8.4 $\pm$ 13)	2.4 $\pm$ 3.2(3.9 $\pm$ 7.4)	5.2 $\pm$ 3.9(7.8 $\pm$ 7.6)
TP $\Gamma_{\text{STRAT}}$ at 70 hPa	-21 $\pm$ 8.3	-22 $\pm$ 8.2	-43	-40 $\pm$ 7.5	n/a	n/a
TP e90 at 70 hPa	26 $\pm$ 9.7	26 $\pm$ 11	52	54 $\pm$ 12	n/a	n/a
NH (SH) POL $\Gamma_{\text{STRAT}}$	-14 $\pm$ 6.9(-11 $\pm$ 6.5)	-13 $\pm$ 8.7(-11 $\pm$ 9.0)	-26(-22)	-24 $\pm$ 8.1(-21 $\pm$ 8.4)	n/a	n/a
NH(SH) POL e90	17 $\pm$ 7.4(17 $\pm$ 10)	17 $\pm$ 7.9(17 $\pm$ 12)	33(34)	32 $\pm$ 8.9 (34 $\pm$ 12)	n/a	n/a
NH(SH) $\Psi^* _{\text{trop}}$	-7.7 $\pm$ -4.4 (2.9 $\pm$ 4.4)	-7.2 $\pm$ -4.3(2.6 $\pm$ 3.6)	-14 (5.1)	-4.9 $\pm$ -4.6 (9.2 $\pm$ -3.3)	0.6 $\pm$ 3.8(1.5 $\pm$ -1.8)	-4.1 $\pm$ 2.5(1.2 $\pm$ -1.6)
TP tropopause	-6.3 $\pm$ 1.8	-6.3 $\pm$ 2.0	-13	-13 $\pm$ 2.1	-0.6 $\pm$ 0.7	-0.8 $\pm$ 0.7
ETP NH(SH) tropopause	-4.1 $\pm$ 1.3(-4.2 $\pm$ 1.3)	-4.3 $\pm$ 1.3(-4.1 $\pm$ 1.3)	-8.7(-8.2)	-8.9 $\pm$ 1.4(-9.4 $\pm$ 1.4)	-0.7 $\pm$ 1.0 (-0.8 $\pm$ 0.9)	-2.3 $\pm$ 1.0(-2.1 $\pm$ 0.7)
NH(SH) MCFLX	-2.9 $\pm$ 1.7(-5.6 $\pm$ 1.6)	-2.5 $\pm$ 1.6(-5.4 $\pm$ 1.5)	-5.0(-11)	-12 $\pm$ 1.7 (-10 $\pm$ 1.6)	-2.8 $\pm$ 0.61 (-2.9 $\pm$ 0.7)	-6.4 $\pm$ 0.7(-5.7 $\pm$ 0.7)
ARC $\chi_{\text{NH},5}$ at 500 hPa	-5.1 $\pm$ 2.2	-5.3 $\pm$ 2.2	-11	-7.1 $\pm$ 2.2	n/a	n/a
ARC $\chi_{\text{NH},50}$ at 500 hPa	-1.6 $\pm$ 0.8	-1.6 $\pm$ 0.9	-3.2	-2.8 $\pm$ 0.9	n/a	n/a



1096

**References**

- 1097 Abalos, M., Orbe, C., Kinnison, D. E., Plummer, D., Oman, L. D., Jöckel, P.,  
 1098 ... others (2019). Future trends in stratosphere-to-troposphere trans-  
 1099 port in CCMi models. *Atmospheric Chemistry and Physics (ACP)*. doi:  
 1100 10.5194/acp-2019-581
- 1101 Abalos, M., Randel, W. J., Kinnison, D. E., & Garcia, R. R. (2017). Using the  
 1102 artificial tracer e90 to examine present and future UTLS tracer transport in  
 1103 WACCM. *Journal of the Atmospheric Sciences*, *74*(10), 3383–3403.
- 1104 Andrews, A. E., Boering, K. A., Daube, B. C., Wofsy, S. C., Loewenstein, M., Jost,  
 1105 H., ... others (2001). Mean ages of stratospheric air derived from in situ  
 1106 observations of CO<sub>2</sub>, CH<sub>4</sub>, and N<sub>2</sub>O. *Journal of Geophysical Research: Atmo-*  
 1107 *spheres*, *106*(D23), 32295–32314.
- 1108 Andrews, D. G., Leovy, C. B., & Holton, J. R. (1987). *Middle Atmosphere Dynam-*  
 1109 *ics*. Academic Press.
- 1110 Appenzeller, C., Holton, J. R., & Rosenlof, K. H. (1996). Seasonal variation of  
 1111 mass transport across the tropopause. *Journal of Geophysical Research: Atmo-*  
 1112 *spheres*, *101*(D10), 15071–15078.
- 1113 Ayarzagüena, B., Charlton-Perez, A. J., Butler, A. H., Hitchcock, P., Simpson, I. R.,  
 1114 Polvani, L. M., ... others (2020). Uncertainty in the response of sudden  
 1115 stratospheric warmings and stratosphere-troposphere coupling to quadrupled  
 1116 CO<sub>2</sub> concentrations in CMIP6 models. *Journal of Geophysical Research: At-*  
 1117 *mospheres*, e2019JD032345.
- 1118 Boering, K. A., Wofsy, S. C., Daube, B. C., Schneider, H. R., Loewenstein, M.,  
 1119 Podolske, J. R., & Conway, T. J. (1996). Stratospheric mean ages and trans-  
 1120 port rates from observations of carbon dioxide and nitrous oxide. *Science*,  
 1121 *274*(5291), 1340–1343.
- 1122 Bönisch, H., Engel, A., Curtius, J., Birner, T., & Hoor, P. (2009). Quantifying trans-  
 1123 port into the lowermost stratosphere using simultaneous in-situ measurements  
 1124 of SF<sub>6</sub> and CO<sub>2</sub>. *Atmos. Chem. Phys*, *9*(16), 5905–5919.
- 1125 Bushell, A. C., Anstey, J. A., Butchart, N., Kawatani, Y., Osprey, S. M., Richter,  
 1126 J. H., ... Yukimoto, S. (2020). Evaluation of the Quasi-Biennial Oscillation in  
 1127 global climate models for the SPARC QBO-initiative. *Quarterly Journal of the*  
 1128 *Royal Meteorological Society*, 1–31. doi: 10.1002/qj.3765
- 1129 Butchart, N., Cionni, I., Eyring, V., Shepherd, T. G., Waugh, D. W., Akiyoshi, H.,  
 1130 ... others (2010). Chemistry–climate model simulations of twenty-first century  
 1131 stratospheric climate and circulation changes. *Journal of Climate*, *23*(20),  
 1132 5349–5374.
- 1133 Butchart, N., & Scaife, A. A. (2001). Removal of chlorofluorocarbons by increased  
 1134 mass exchange between the stratosphere and troposphere in a changing cli-  
 1135 mate. *Nature*, *410*(6830), 799–802.
- 1136 CCMVal, S. (2010). *SPARC report on the evaluation of chemistry-climate mod-*  
 1137 *els*, Edited by: Eyring, V., Shepherd, T.G., and Waugh, D.W. (Tech. Rep.).  
 1138 SPARC report.
- 1139 Chemke, R., & Polvani, L. M. (2019). Exploiting the abrupt 4×CO<sub>2</sub> scenario to elu-  
 1140 cidate tropical expansion mechanisms. *Journal of Climate*, *32*(3), 859–875.
- 1141 Chiodo, G., & Polvani, L. M. (2017). Reduced Southern Hemispheric circulation  
 1142 response to quadrupled CO<sub>2</sub> due to stratospheric ozone feedback. *Geophysical*  
 1143 *Research Letters*, *44*(1), 465–474.
- 1144 Chipperfield, M. P., Dhomse, S., Hossaini, R., Feng, W., Santee, M. L., Weber, M.,  
 1145 ... Coldewey-Egbers, M. (2018). On the cause of recent variations in lower  
 1146 stratospheric ozone. *Geophysical Research Letters*, *45*(11), 5718–5726.
- 1147 Danielsen, E. F. (1993). In situ evidence of rapid, vertical, irreversible transport  
 1148 of lower tropospheric air into the lower tropical stratosphere by convective  
 1149 cloud turrets and by larger-scale upwelling in tropical cyclones. *Journal of*  
 1150 *Geophysical Research: Atmospheres*, *98*(D5), 8665–8681.

- 1151 Del Genio, A. D., Yao, M.-S., & Jonas, J. (2007). Will moist convection be stronger  
1152 in a warmer climate? *Geophysical Research Letters*, *34*(16). doi: 10.1029/  
1153 2007GL030525
- 1154 Doherty, R. M., Orbe, C., Zeng, G., Plummer, D. A., Prather, M. J., Wild, O., ...  
1155 Mackenzie, I. A. (2017). Multi-model impacts of climate change on pollution  
1156 transport from global emission source regions. *Atmospheric Chemistry and  
1157 Physics*, *17*(23), 14219–14237.
- 1158 Eichinger, R., Garny, H., Šácha, P., Danker, J., Dietmüller, S., & Oberländer-Hayn,  
1159 S. (2020). Effects of missing gravity waves on stratospheric dynamics; Part 1:  
1160 Climatology. *Climate Dynamics*, *54*(5), 3165–3183.
- 1161 Engel, A., Möbius, T., Bönisch, H., Schmidt, U., Heinz, R., Levin, I., ... others  
1162 (2009). Age of stratospheric air unchanged within uncertainties over the past  
1163 30 years. *Nature Geoscience*, *2*(1), 28–31.
- 1164 Eyring, V., Bony, S., Meehl, G. A., Senior, C. A., Stevens, B., Stouffer, R. J., &  
1165 Taylor, K. E. (2016). Overview of the Coupled Model Intercomparison Project  
1166 Phase 6 (CMIP6) experimental design and organization. *Geoscientific Model  
1167 Development*, *9*, 1937–1958. doi: 10.5194/gmd-9-1937-2016
- 1168 Eyring, V., Butchart, N., Waugh, D. W., Akiyoshi, H., Austin, J., Bekki, S., ... oth-  
1169 ers (2006). Assessment of temperature, trace species, and ozone in chemistry-  
1170 climate model simulations of the recent past. *Journal of Geophysical Research:  
1171 Atmospheres*, *111*. doi: 10.1029/2006JD007327
- 1172 Eyring, V., Lamarque, J.-F., Hess, P., Arfeuille, F., Bowman, K., Chipperfield, M. P.,  
1173 ... others (2013). Overview of IGAC/SPARC Chemistry-Climate Model  
1174 Initiative (CCMI) community simulations in support of upcoming ozone and  
1175 climate assessments. *SPARC Newsletter*, *40*(January), 48–66.
- 1176 Fang, Y., Fiore, A. M., Horowitz, L. W., Gnanadesikan, A., Held, I., Chen, G., ...  
1177 Levy, H. (2011). The impacts of changing transport and precipitation on  
1178 pollutant distributions in a future climate. *Journal of Geophysical Research:  
1179 Atmospheres*, *116*(D18).
- 1180 Fioletov, V. E., Bodeker, G. E., Miller, A. J., McPeters, R. D., & Stolarski, R.  
1181 (2002). Global and zonal total ozone variations estimated from ground-based  
1182 and satellite measurements: 1964–2000. *Journal of Geophysical Research:  
1183 Atmospheres*, *107*(D22). doi: 10.1029/2001JD001350
- 1184 Garcia, R. R., & Randel, W. J. (2008). Acceleration of the Brewer-Dobson circula-  
1185 tion due to increases in greenhouse gases. *Journal of the Atmospheric Sciences*,  
1186 *65*(8), 2731–2739.
- 1187 Geller, L. S., Elkins, J. W., Lobert, J. M., Clarke, A. D., Hurst, D. F., Butler, J. H.,  
1188 & Myers, R. C. (1997). Tropospheric SF<sub>6</sub>: Observed latitudinal distribution  
1189 and trends, derived emissions and interhemispheric exchange time. *Geophysical  
1190 Research Letters*, *24*(6), 675–678.
- 1191 Gerber, E. P., Butler, A., Calvo, N., Charlton-Perez, A., Giorgetta, M., Manzini,  
1192 E., ... others (2012). Assessing and understanding the impact of strato-  
1193 spheric dynamics and variability on the earth system. *Bulletin of the American  
1194 Meteorological Society*, *93*(6), 845–859.
- 1195 Gettelman, A., & Sobel, A. H. (2000). Direct diagnoses of stratosphere–troposphere  
1196 exchange. *Journal of the Atmospheric Sciences*, *57*(1), 3–16.
- 1197 Grise, K. M., & Polvani, L. M. (2016). Is climate sensitivity related to dynami-  
1198 cal sensitivity? *Journal of Geophysical Research: Atmospheres*, *121*(10), 5159–  
1199 5176.
- 1200 Grooß, J.-U., & Russell, J. M. (2005, October). Technical note: A stratospheric  
1201 climatology for O<sub>3</sub>, H<sub>2</sub>O, CH<sub>4</sub>, NO<sub>x</sub>, HCl and HF derived from HALOE mea-  
1202 surements. *Atmospheric Chemistry and Physics*, *5*(10), 2797–2807. doi:  
1203 10.5194/acp-5-2797-2005
- 1204 Hall, T. M., & Plumb, R. A. (1994). Age as a diagnostic of stratospheric transport.  
1205 *Journal of Geophysical Research: Atmospheres*, *99*(D1), 1059–1070.

- 1206 Hall, T. M., & Waugh, D. W. (2000). Stratospheric residence time and its relation-  
 1207 ship to mean age. *Journal of Geophysical Research: Atmospheres*, *105*(D5),  
 1208 6773–6782.
- 1209 Hall, T. M., Waugh, D. W., Boering, K. A., & Plumb, R. A. (1999). Evaluation  
 1210 of transport in stratospheric models. *Journal of Geophysical Research: Atmo-*  
 1211 *spheres*, *104*(D15), 18815–18839.
- 1212 Hardiman, S. C., Butchart, N., & Calvo, N. (2014). The morphology of the Brewer-  
 1213 Dobson circulation and its response to climate change in CMIP5 simulations.  
 1214 *Quarterly Journal of the Royal Meteorological Society*, *140*(683), 1958–1965.
- 1215 Held, I. M., & Soden, B. J. (2006). Robust responses of the hydrological cycle to  
 1216 global warming. *Journal of climate*, *19*(21), 5686–5699.
- 1217 Hess, P. G. (2005). A comparison of two paradigms: The relative global roles of  
 1218 moist convective versus nonconvective transport. *Journal of Geophysical Re-*  
 1219 *search: Atmospheres*, *110*(D20). doi: 10.1029/2004JD005456
- 1220 Holton, J. R., & Gettelman, A. (2001). Horizontal transport and the dehydration of  
 1221 the stratosphere. *Geophysical Research Letters*, *28*(14), 2799–2802.
- 1222 Holzer, M., & Boer, G. J. (2001). Simulated changes in atmospheric transport cli-  
 1223 mate. *Journal of Climate*, *14*(23), 4398–4420.
- 1224 Holzer, M., & Hall, T. M. (2000). Transit-time and tracer-age distributions in geo-  
 1225 physical flows. *Journal of the Atmospheric Sciences*, *57*(21), 3539–3558.
- 1226 Holzer, M., Orbe, C., & Primeau, F. W. (2012). Stratospheric mean residence time  
 1227 and mean age on the tropopause: Connections and implications for observa-  
 1228 tional constraints. *Journal of Geophysical Research: Atmospheres*, *117*(D12).
- 1229 Johnston, H. (1989). Evaluation of excess carbon 14 and strontium 90 data for  
 1230 suitability to test two-dimensional stratospheric models. *Journal of Geophysi-*  
 1231 *cal Research: Atmospheres*, *94*(D15), 18485–18493.
- 1232 Kelley, M., Schmidt, G. A., Nazarenko, L. S., Bauer, S. E., Ruedy, R., Russell,  
 1233 G. L., . . . others (2019). GISS-e2. 1: Configurations and climatology. *Journal*  
 1234 *of Advances in Modeling Earth Systems*, e2019MS002025.
- 1235 Kim, D., Del Genio, A. D., & Yao, M.-S. (2013). Moist convection scheme in Model  
 1236 E2. *arXiv preprint arXiv:1312.7496*.
- 1237 Klonecki, A., Hess, P., Emmons, L., Smith, L., Orlando, J., & Blake, D. (2003). Sea-  
 1238 sonal changes in the transport of pollutants into the arctic troposphere-model  
 1239 study. *Journal of Geophysical Research: Atmospheres*, *108*(D4).
- 1240 Lee, Y., Lamarque, J., Flanner, M., Jiao, C., Shindell, D., Berntsen, T., . . . others  
 1241 (2013). Evaluation of preindustrial to present-day black carbon and its albedo  
 1242 forcing from Atmospheric Chemistry and Climate Model Intercomparison  
 1243 Project (ACCMIP). *Atmospheric Chemistry and Physics*, *13*(5), 2607–2634.
- 1244 Levin, I., & Hesshaimer, V. (1996). Refining of atmospheric transport model entries  
 1245 by the globally observed passive tracer distributions of <sup>85</sup>krypton and sulfur  
 1246 hexafluoride (SF<sub>6</sub>). *Journal of Geophysical Research: Atmospheres*, *101*(D11),  
 1247 16745–16755.
- 1248 Li, F., Austin, J., & Wilson, J. (2008). The strength of the Brewer-Dobson circula-  
 1249 tion in a changing climate: Coupled chemistry–climate model simulations.  
 1250 *Journal of Climate*, *21*(1), 40–57.
- 1251 Li, F., Stolarski, R. S., Pawson, S., Newman, P. A., & Waugh, D. (2010). Narrowing  
 1252 of the upwelling branch of the Brewer-Dobson circulation and Hadley Cell in  
 1253 chemistry-climate model simulations of the 21<sup>st</sup> century. *Geophysical Research*  
 1254 *Letters*, *37*(13).
- 1255 Lindzen, R. (1984). Gravity waves in the mesosphere. *Dynamics of the Middle At-*  
 1256 *mosphere*, *3*, 18.
- 1257 Lorenz, D. J., & DeWeaver, E. T. (2007). Tropopause height and zonal wind re-  
 1258 sponse to global warming in the IPCC scenario integrations. *Journal of Geo-*  
 1259 *physical Research: Atmospheres*, *112*(D10).
- 1260 Lu, J., Chen, G., & Frierson, D. M. W. (2008). Response of the zonal mean at-

- 1261           mospheric circulation to El Niño versus global warming. *Journal of Climate*,  
1262           *21*(22), 5835–5851.
- 1263 Marvel, K., Schmidt, G. A., Shindell, D., Bonfils, C., LeGrande, A. N., Nazarenko,  
1264           L., & Tsigaridis, K. (2015). Do responses to different anthropogenic forcings  
1265           add linearly in climate models? *Environmental Research Letters*, *10*(10),  
1266           104010.
- 1267 McPeters, R., Kroon, M., Labow, G., Brinksma, E., Balis, D., Petropavlovskikh, I.,  
1268           ... Levelt, P. (2008). Validation of the Aura ozone monitoring instrument  
1269           total column ozone product. *Journal of Geophysical Research: Atmospheres*,  
1270           *113*(D15).
- 1271 McPeters, R. D., Bhartia, P., Haffner, D., Labow, G. J., & Flynn, L. (2013). The  
1272           version 8.6 sbuv ozone data record: An overview. *Journal of Geophysical Re-*  
1273           *search: Atmospheres*, *118*(14), 8032–8039.
- 1274 Menzel, M. E., Waugh, D., & Grise, K. (2019). Disconnect between Hadley cell and  
1275           subtropical jet variability and response to increased CO<sub>2</sub>. *Geophysical Research*  
1276           *Letters*, *46*(12), 7045–7053.
- 1277 Mote, P. W., Rosenlof, K. H., McIntyre, M. E., Carr, E. S., Gille, J. C., Holton,  
1278           J. R., ... Waters, J. W. (1996). An atmospheric tape recorder: The imprint  
1279           of tropical tropopause temperatures on stratospheric water vapor. *Journal of*  
1280           *Geophysical Research: Atmospheres*, *101*(D2), 3989–4006.
- 1281 Murray, L. T., Mickley, L. J., Kaplan, J. O., Sofen, E. D., Pfeiffer, M., & Alexan-  
1282           der, B. (2014). Factors controlling variability in the oxidative capacity of  
1283           the troposphere since the last glacial maximum. *Atmospheric Chemistry and*  
1284           *Physics*.
- 1285 Neu, J. L., & Plumb, R. A. (1999). Age of air in a leaky pipe model of stratospheric  
1286           transport. *Journal of Geophysical Research: Atmospheres*, *104*(D16), 19243–  
1287           19255.
- 1288 Oberländer, S., Langematz, U., & Meul, S. (2013). Unraveling impact factors for  
1289           future changes in the Brewer-Dobson circulation. *Journal of Geophysical Re-*  
1290           *search: Atmospheres*, *118*(18), 10–296.
- 1291 O’Gorman, P. A., & Schneider, T. (2008). The hydrological cycle over a wide range  
1292           of climates simulated with an idealized gcm. *Journal of Climate*, *21*(15), 3815–  
1293           3832.
- 1294 Oman, L., Waugh, D. W., Pawson, S., Stolarski, R. S., & Newman, P. A. (2009). On  
1295           the influence of anthropogenic forcings on changes in the stratospheric mean  
1296           age. *Journal of Geophysical Research: Atmospheres*, *114*(D3).
- 1297 Orbe, C., Holzer, M., & Polvani, L. M. (2012). Flux distributions as robust diag-  
1298           nostics of stratosphere-troposphere exchange. *Journal of Geophysical Research:*  
1299           *Atmospheres*, *117*(D1).
- 1300 Orbe, C., Holzer, M., Polvani, L. M., & Waugh, D. (2013). Air-mass origin as a  
1301           diagnostic of tropospheric transport. *Journal of Geophysical Research: Atmo-*  
1302           *spheres*, *118*(3), 1459–1470.
- 1303 Orbe, C., Newman, P. A., Waugh, D. W., Holzer, M., Oman, L. D., Li, F., &  
1304           Polvani, L. M. (2015). Air-mass origin in the Arctic. Part II: Response to  
1305           increases in greenhouse gases. *Journal of Climate*, *28*(23), 9105–9120.
- 1306 Orbe, C., Oman, L. D., Strahan, S. E., Waugh, D. W., Pawson, S., Takacs, L. L., &  
1307           Molod, A. M. (2017). Large-scale atmospheric transport in GEOS replay simu-  
1308           lations. *Journal of Advances in Modeling Earth Systems*, *9*(7), 2545–2560.
- 1309 Orbe, C., Roedel, L. V., Adames, A. F., Dezfuli, A., Fasullo, J., Gleckler, P. J., ...  
1310           Schmidt, G. A. (2020). Current Representation of Modes of Variability in 6  
1311           U.S. Climate Models. *Journal of Climate*. (Submitted)
- 1312 Orbe, C., Waugh, D. W., Newman, P. A., & Steenrod, S. (2016). The transit-time  
1313           distribution from the Northern Hemisphere midlatitude surface. *Journal of the*  
1314           *Atmospheric Sciences*, *73*(10), 3785–3802.
- 1315 Orbe, C., Yang, H., Waugh, D., Zeng, G., Morgenstern, O., Kinnison, D., ... others

- 1316 (2019). Large-scale tropospheric transport in the Chemistry-Climate Model  
1317 Initiative (CCMI) simulations. *Atmos. Chem. Phys.*, *18*, 7217–7235.
- 1318 Plumb, R. A. (2002). Stratospheric transport. *Journal of the Meteorological Society*  
1319 *of Japan. Ser. II*, *80*(4B), 793–809.
- 1320 Polvani, L. M., Abalos, M., Garcia, R., Kinnison, D., & Randel, W. J. (2018). Sig-  
1321 nificant weakening of Brewer-Dobson circulation trends over the 21<sup>st</sup> century  
1322 as a consequence of the Montreal Protocol. *Geophysical Research Letters*,  
1323 *45*(1), 401–409.
- 1324 Polvani, L. M., Waugh, D. W., Correa, G. J., & Son, S.-W. (2011). Stratospheric  
1325 ozone depletion: The main driver of twentieth-century atmospheric circulation  
1326 changes in the Southern Hemisphere. *Journal of Climate*, *24*(3), 795–812.
- 1327 Prather, M. J., & Remsberg, E. E. (1993). The atmospheric effects of stratospheric  
1328 aircraft. report of the 1992 models and measurements workshop. volume 3:  
1329 Special diagnostic studies.
- 1330 Randel, W. J., Wu, F., Oltmans, S. J., Rosenlof, K., & Nedoluha, G. E. (2004).  
1331 Interannual changes of stratospheric water vapor and correlations with trop-  
1332 ical tropopause temperatures. *Journal of the Atmospheric Sciences*, *61*(17),  
1333 2133–2148.
- 1334 Rani, K. P., Chandrashekhara, M., & Paramesh, L. (2014). Vertical profile of radon  
1335 and its progeny concentrations and its effect on atmospheric electrical con-  
1336 ductivity near the surface of the earth. *International Journal of Advanced*  
1337 *Scientific and Technical Research*, *4*(4).
- 1338 Richter, J. H., Butchart, N., Kawatani, Y., Bushell, A. C., Holt, L., Serva, F., ...  
1339 others (2019). Response of the Quasi-Biennial Oscillation to a warming cli-  
1340 mate in global climate models. *Quarterly Journal of the Royal Meteorological*  
1341 *Society*.
- 1342 Rind, D., Jonas, J., Balachandran, N. K., Schmidt, G. A., & Lean, J. (2014). The  
1343 QBO in two GISS global climate models: 1. Generation of the QBO. *Journal*  
1344 *of Geophysical Research: Atmospheres*, *119*(14), 8798–8824.
- 1345 Rind, D., Lerner, J., Perlwitz, J., McLinden, C., & Prather, M. (2002). Sensitivity of  
1346 tracer transports and stratospheric ozone to sea surface temperature patterns  
1347 in the doubled CO<sub>2</sub> climate. *Journal of Geophysical Research: Atmospheres*,  
1348 *107*(D24), ACL–25.
- 1349 Rind, D., Lerner, J., Shah, K., & Suozzo, R. (1999). Use of on-line tracers as a diag-  
1350 nostic tool in general circulation model development: 2. Transport between the  
1351 troposphere and stratosphere. *Journal of Geophysical Research: Atmospheres*,  
1352 *104*(D8), 9151–9167.
- 1353 Rind, D., Orbe, C., Jonas, J., Nazarenko, L., Zhou, T., Kelley, M., ... Tausnev,  
1354 N. (2020). Giss model e2.2: A climate model optimized for the middle atmo-  
1355 sphere. part 1: Model structure, climatology, variability and climate sensitivity.  
1356 *J. Geophys. Res. Atmos.*. doi: 10.1029/2019JD032204
- 1357 Rind, D., Shindell, D., Lonergan, P., & Balachandran, N. K. (1998). Climate change  
1358 and the middle atmosphere. Part III: The doubled CO<sub>2</sub> climate revisited.  
1359 *Journal of Climate*, *11*(5), 876–894.
- 1360 Rind, D., Suozzo, R., Balachandran, N. K., Lacis, A., & Russell, G. (1988). The  
1361 GISS global climate-middle atmosphere model. Part I: Model structure and  
1362 climatology. *Journal of the Atmospheric Sciences*, *45*(3), 329–370.
- 1363 Scaife, A. A., Karpechko, A. Y., Baldwin, M. P., Brookshaw, A., Butler, A. H.,  
1364 Eade, R., ... others (2016). Seasonal winter forecasts and the stratosphere.  
1365 *Atmospheric Science Letters*, *17*(1), 51–56.
- 1366 Schoeberl, M., Douglass, A., Newman, P., Lait, L., Lary, D., Waters, J., ... oth-  
1367 ers (2008). Qbo and annual cycle variations in tropical lower stratosphere  
1368 trace gases from HALOE and Aura MLS observations. *Journal of Geophysical*  
1369 *Research: Atmospheres*, *113*(D5).
- 1370 Seviour, W. J. M., Hardiman, S. C., Gray, L. J., Butchart, N., MacLachlan, C., &

- 1371 Scaife, A. A. (2014). Skillful seasonal prediction of the southern annular mode  
1372 and Antarctic ozone. *Journal of Climate*, *27*(19), 7462–7474.
- 1373 Sherwood, S. C., & Dessler, A. E. (2000). On the control of stratospheric humidity.  
1374 *Geophysical Research Letters*, *27*(16), 2513–2516.
- 1375 Shindell, D. T., Pechony, O., Voulgarakis, A., Faluvegi, G., Nazarenko, L., Lamar-  
1376 que, J.-F., . . . Schmidt, G. A. (2013, March). Interactive ozone and methane  
1377 chemistry in GISS-e2 historical and future climate simulations. *Atmospheric*  
1378 *Chemistry and Physics*, *13*(5), 2653–2689. Retrieved from [https://doi.org/](https://doi.org/10.5194/acp-13-2653-2013)  
1379 [10.5194/acp-13-2653-2013](https://doi.org/10.5194/acp-13-2653-2013) doi: 10.5194/acp-13-2653-2013
- 1380 Sigmond, M., Siegmund, P. C., Manzini, E., & Kelder, H. (2004). A simulation  
1381 of the separate climate effects of middle-atmospheric and tropospheric CO<sub>2</sub>  
1382 doubling. *Journal of climate*, *17*(12), 2352–2367.
- 1383 Tweedy, O. V., Kramarova, N. A., Strahan, S. E., Newman, P. A., Coy, L., Ran-  
1384 del, W. J., . . . Frith, S. M. (2017). Response of trace gases to the disrupted  
1385 2015–2016 Quasi-Biennial Oscillation. *Atmospheric Chemistry & Physics*,  
1386 *17*(11).
- 1387 Vecchi, G. A., & Soden, B. J. (2007). Global warming and the weakening of the  
1388 tropical circulation. *Journal of Climate*, *20*(17), 4316–4340.
- 1389 Waugh, D. W., Crotwell, A. M., Dlugokencky, E. J., Dutton, G. S., Elkins, J. W.,  
1390 Hall, B. D., . . . others (2013). Tropospheric SF<sub>6</sub>: Age of air from the Northern  
1391 Hemisphere midlatitude surface. *Journal of Geophysical Research: Atmo-*  
1392 *spheres*, *118*(19), 11–429.
- 1393 Yang, H., Waugh, D. W., Orbe, C., Patra, P. K., Jöckel, P., Lamarque, J.-F., . . .  
1394 Dlugokencky, E. J. (2019). Evaluating simulations of interhemispheric trans-  
1395 port: Interhemispheric exchange time versus SF<sub>6</sub> age. *Geophysical Research*  
1396 *Letters*, *46*(2), 1113–1120.
- 1397 Yoo, C., & Son, S.-W. (2016). Modulation of the boreal wintertime Madden-Julian  
1398 Oscillation by the stratospheric Quasi-Biennial Oscillation. *Geophysical Re-*  
1399 *search Letters*, *43*(3), 1392–1398.